CHAPTER 4

Peptidic stabilization of gold nanorods

4.1 Abstract

Gold nanorods (GNRs) are a particularly interesting class of nanoparticles: their dimensions can be tuned to produce rods of different aspect ratios (a.r.) providing well-defined optical properties due to the localized surface plasmon resonance (LSPR) position. GNRs are commonly employed in nanophotonics, biosensing, and surface-enhanced Raman scattering (SERS) applications, and they are also believed to have different effects in immunological and biomedical applications when compared to spherical gold nanoparticles (GNPs). However, the wider use of GNRs is restricted due to difficulties associated with their surface stabilization. Reagents that are used as stabilizers during GNR synthesis are toxic, and need to be displaced from the gold surface before being employed in biological applications. Polymer or silica coatings commonly employed to stabilize GNRs are typically thick (>10 nm), negatively affecting the use of GNRs in applications based on their optical properties. Previously, it was shown that peptide amphiphiles effectively stabilized spherical GNPs in the 20-100 nm size range. The peptide amphiphiles formed a self-assembled monolayer (SAM) on the gold surface with a thickness of <5 nm. In this chapter, the use of peptide amphiphiles as a stabilizing coating for GNRs is reported. The procedure reported for peptide amphiphile-stabilized GNPs was optimized for GNR stabilization, resulting in long-term stability and resistance to external factors inducing aggregation. Moreover, the formed SAMs were probed for their secondary structure distribution and coverage density. All tested peptide amphiphiles formed dense (2.62-3.87 peptides/nm^2) and highly ordered (51.8-58.8% β-content) shells on the GNR surface. Due to their high stability and thin coating, peptide amphiphile-stabilized GNRs are of particular interest as a tool in biophysical and biomedical applications.

4.2 Introduction

Gold nanorods (GNRs) first emerged in 1999 and provided an opportunity to synthesize asymmetric nanoparticles with finely tunable physical dimensions and optical properties.[1-4] The GNR aspect ratio (a.r.), which is the relationship between their length and width, defines the optical properties of these nanoparticles and is reflected in the localized surface plasmon resonance (LSPR) position. The LSPR can therefore vary between 600 nm and 1200 nm. Also, due to the fact that the LSPR position is in the near-infrared (NIR) region of the electromagnetic spectrum, outside of the region where water and biological molecules absorb, GNRs are considered to be highly suitable for biological applications. Upon excitation with a laser matching their plasmon frequency, these nanoparticles emit an enhanced multiphoton signal. GNRs have been extensively used as extraordinarily bright substrates for *in vitro* and *in vivo* two-photon (2P) luminescence imaging that minimizes the damage to biological samples and prolongs imaging time.[5-9] GNRs have also been utilized as contrast agents in photoacoustic imaging,[10] and other SPR-enhanced imaging and detection techniques.[7, 11, 12] In addition, GNRs are insensitive to photobleaching,[13] provide a 3D spatial resolution of the read-out signal,[5] and their spatial orientation can be deduced from their polarized light scattering.[14] GNR excitation can also result in the conversion of optical energy into heat, therefore GNRs are used in cancer photothermal therapy.[7, 15, 16] Finally, GNR optical properties are extremely sensitive to changes in the environment which is especially attractive for label-free bio-sensor development.[17, 18]

The shape of GNRs, which gives rise to their unique optical properties, is achieved *via* seed-mediated growth in the presence of silver nitrate ($AgNO_3$)

and high excesses of specific cationic surfactants such as cetyltrimethylammonium bromide (CTAB),[19] cetyltrimethylammonium chloride (CTAC),[20] benzyldimethylhexadecylammonium chloride (BDAC), or mixtures thereof.[3] These molecules form a bilayer on the gold surface and are essential for the shape control and stability of GNRs. These non-covalent interactions are weak enough to allow surface modification of GNRs *via* displacement of the surfactant. Moreover, due to the cationic and amphiphilic nature of these molecules, surfactant-protected GNRs are unstable under physiological conditions and cause severe cytotoxicity.[12] Displacement of CTAB is achieved through common nanoparticle stabilization approaches including polymer coating (*e.g.* thiolated PEG molecules[21, 22] and other polymers[23]), silica condensation,[24] or alternatively, CTAB can be replaced by thiolated analogues.[25, 26] The first two methods rely on creating a steric barrier between individual GNRs. Thiolated PEGs displace CTAB *via* ligand exchange and form a shell attached to the gold surface through Au-S bonds. It was shown that 5-10 kDa thiolated PEGs are optimal for stabilization of GNRs.[21] This PEG size corresponds to a substantial contour length: at least 30 nm and longer for a fully "stretched" molecule.[27, 28] Silica precursors can condense on the GNR surface, but the resulting coatings are typically thick as well (>10 nm).[29]

GNRs are utilized to study ligand-receptor interactions, and hence the choice of the protective molecule is crucial. The formed shell has to meet several requirements: (i) be suitable for further functionalization with a ligand of interest; (ii) be of minimal thickness to allow detection of biomolecule interactions close to the GNR surface. Since the LSPR is defined by the local refractive index close to the particle's surface, the studied interactions should take place as close to the gold surface as possible. This way the shift of LSPR band is a direct measure of such interactions.[18] Also, when *in vitro* or

in vivo applications are envisioned, a significant increase in GNR dimensions due to the presence of a shell can alter the pathways by which the nanoparticles are taken up by cells and cleared from the blood stream. From this point of view the common stabilization approaches are not ideal and a new stabilization method is desired. In this chapter thiolated peptide amphiphiles are studied as potential GNR stabilizers. These amphiphiles comprise a beta-sheet forming peptide domain conjugated, at the N-terminus, to a thiolated alkyl chain. The presence of the alkyl chain is likely to lead to increased stability as it was previously shown that conjugation of thiolated PEG (2000 Da) with 11-mercaptoundecanoic acid (MUA) improved the stability of the resulting GNR conjugates.[22] Additionally, the coverage densities increased from <1 to up to 3.3 molecules/nm^2. This was attributed to better penetration of the hydrophobic tails into the CTAB bilayer in comparison to the hydrophilic thiolated PEGs. It was also shown that use of a thiolated analogue of CTAB, 16-mercaptohexadecyl-trimethylammonium bromide (MTAB), improved the ligand density from 0.9 (± 0.2) to 3.6 (± 1.0) molecules/nm^2.[24] Interestingly, MTAB formed a uniform monolayer at the GNR surface, while CTAB coatings are less dense at the rod tips. Also, no significant difference in MTAB coverage was detected for GNRs of different a.r. (1.4, 2.3, 3.2, and 3,9 respectively).[26] These findings emphasize the importance of a thiolated alkyl chain presence, implying peptide amphiphiles are likely to act as effective stabilizing coatings.

In **Chapter 3** of this thesis, the use of thiolated peptide amphiphiles for stabilization of spherical gold nanoparticles (GNPs) by formation of a self-assembled monomer (SAM) was described.[30] It was shown that peptide amphiphiles stabilized GNPs of different diameters under physiological conditions and at high salt or dithiothreitol (DTT) concentrations. This extraordinary stability of the peptide amphiphile-coated GNPs was attributed

to a combination of effects arising from their amphiphilic nature: firstly, alkyl chains are bound to the gold surface *via* an Au-S bond and create a hydrophobic environment around the core. This depletes the presence of water, and the molecules dissolved in it, from the surface of the GNP. Secondly, peptide self-assembly leads to the formation of a dense self-assembled monolayer (SAM) on the surface of the GNPs. Finally, a correlation between the surface curvature and the stabilizing capacity of the peptide or peptide amphiphile was also implicated in the stabilizing effect.

To probe these stabilizing effects further, the same coating approach was applied to gold nanorods in this chapter. As before, a ligand exchange procedure was used to replace the original CTAB bilayer on the GNR surface with molecules **1-4** (**Scheme 4.1**).[30] As both the shape and the original surface chemistry of GNRs differed from GNPs, this had implications for the ligand exchange as well as for the overall stability that was achieved. The rod-like shape is a combination of high (at the tips) and low (in the center of the rods) curvature areas, while CTAB creates a hydrophobic environment shown to be difficult to penetrate with hydrophilic molecules.[22] Both factors were suggested to contribute to the ligand density and secondary structure distribution within the peptide amphiphile shell attached to the GNR surface. Additionally, the protective capability of the thiolated peptide amphiphiles was simultaneously evaluated and explained though the coated-GNR behavior upon addition of molecules inducing aggregation (high-salt conditions or competition with thiol ligands). UV-Vis spectroscopy (UV-Vis) was used to elucidate the aggregation state of GNRs, while the resulting peptide amphiphile-based SAMs were analyzed with transmission electron microscopy (TEM) and Fourier-transform infrared spectroscopy (FTIR).

4.3 Results and Discussion

4.3.1 Peptide amphiphile design

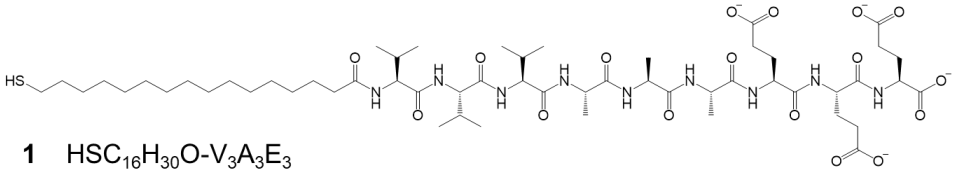

1 $HSC_{16}H_{30}O\text{-}V_3A_3E_3$

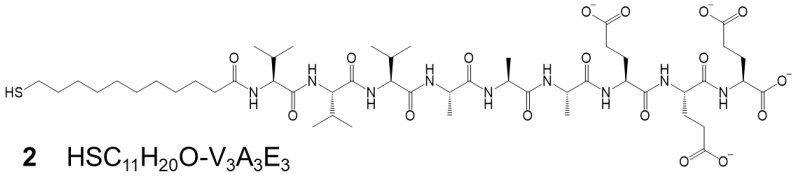

2 $HSC_{11}H_{20}O\text{-}V_3A_3E_3$

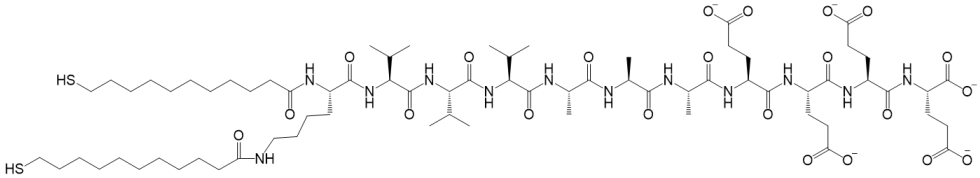

3 $(HSC_{11}H_{20}O)_2\text{-}KV_3A_3E_4$

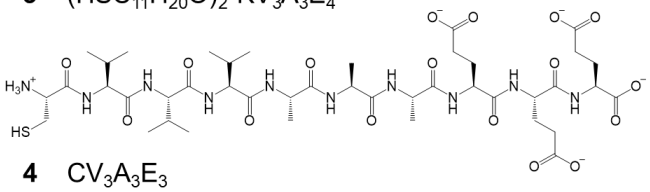

4 $CV_3A_3E_3$

Scheme 4.1. Sequences and structures of peptides and amphiphiles used in this study.

Similar to **Chapter 3** of this thesis, peptide amphiphiles comprising a thiolated alkyl chain of either 16 or 11 carbons in length and a peptide domain with the sequence $V_3A_3E_3$ were designed and synthesized. These are dubbed molecules **1** and **2** respectively (**Scheme 4.1**). A third construct with two C-11 alkyl chains, molecule **3**, possesses increased steric bulk within the hydrophobic domain and was also introduced to probe the effect of a

bidentate binding ligand. The sequence of **3** was extended with a fourth glutamic acid residue (Glu, E) for increased solubility. Peptide **4** contained a cysteine (Cys, C) amino acid instead of a thiolated alkyl chain and served as a reference molecule to study the impact of the hydrophobic alkyl chain domain of **1-3**.

All four molecules are suitable for displacement of citrate from the surface of GNPs, (**Chapter 3** of this thesis) and are therefore likely to be effective for the displacement of CTAB from the surface of GNRs as well. In addition to using molecule **4** as a reference molecule, GNRs were also coated with thiolated PEG-OMe with average molecular weights of 750 and 5000 Da. The reason thiolated PEG-OMe was chosen as a reference stabilizing molecule is that thiolated PEG_{5000} has been reported to be an optimal length for GNR stabilization, while thiolated PEG_{750} was chosen because its shorter contour length (in its extended conformation) is comparable to the length of the peptide amphiphiles used in this study (4.8 nm based on 0.28 nm per -CH_2CH_2O- repeat).[27, 28]

4.3.2 GNR coating protocol optimization

GNRs with an aspect ratio (a.r.) of 3.3 (LSPR 756 nm) were synthesized according to the seed-mediated overgrowth method (**Figure 4.1**). The average dimensions of the resulting rods were 46.4 (± 8.3) by 14.0 (± 2.9) nm. Rods with these dimensions were selected as they are suitable for potential future applications using two-photon microscopy.[18] As-synthesized GNRs were stabilized with a cetyltrimethylammonium bromide (CTAB) bilayer which was displaced from the GNR surface *via* ligand exchange with the thiol-containing ligands **1-4** and thiolated PEGs (750 and 5000 Da).

The thiolated peptide amphiphiles require an optimized coating procedure (**Chapter 3** of this thesis).[30] To prevent the undesired simultaneous formation of peptide amphiphile fibers, **1-3** were dissolved in pure DMSO prior to the ligand exchange, which was performed in aqueous DMSO. Previously, it was shown that ligand exchange between citrate resident on the GNP surface and thiolated peptide amphiphiles was successful in 25% DMSO (aq. v/v) (**Chapter 3** of this thesis): after 1h incubation, the excess ligand was removed *via* a combination of centrifugation and size-exclusion chromatography (SEC). Concomitantly, the medium was replaced with PBS (pH 7.2). The resulting peptide amphiphile-stabilized GNPs were fiber-free and dense well-defined peptide amphiphile monolayers around each gold core were observed with transmission electron microscopy (TEM). However, this approach resulted in a significant red-shift of the SPR band (>20 nm) of the GNRs (**Figure 4.1A**). TEM analysis indicated that this red-shift was caused by the presence of associated peptide amphiphile fibers, although coated GNRs were individually coated and separated from each other (**Figure 4.1B**). Fiber formation was particularly prevalent when **1** and **3** were used, while rods coated with **2** (**GNR@2**) were typically free of fibers. This was attributed to the different alkyl chain lengths, resulting in different fiber formation kinetics and critical fiber formation concentrations. Reduction of the alkyl chain length from C16 to C11 results in a slower fiber formation rate and a higher critical concentration in the case of **2** (**Chapter 2** of this thesis). Since free residual fibers could affect applications and stability of the coated GNRs, we optimized the coating procedure in order to obtain pure GNRs coated with **1** (**GNR@1**) or **3** (**GNR@3**) in the absence of peptide amphiphile fibers.

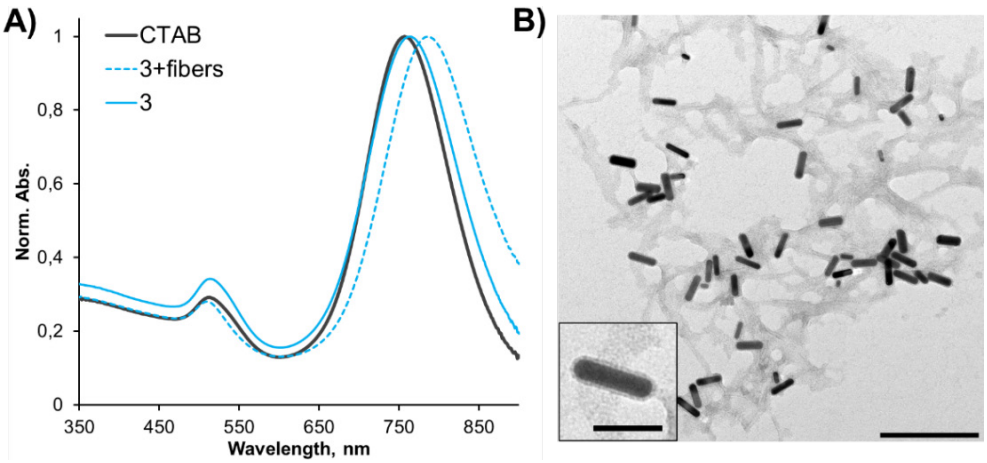

Figure 4.1. Optimization of the GNR coating procedure with molecule **3** (A) UV-Vis spectra of a **GNR@3** sample with associated fibers (dashed line) and a fiber-free sample (solid blue line), compared to the original CTAB-coated GNRs (black line); (B) a representative TEM image of fibers associated with **GNR@3**. TEM image: scale bar is 200 nm (insert - 50 nm); 0.5% uranyl acetate staining.

Fiber formation in solution can be disrupted or delayed if an appropriate solvent is added.[31] As DMSO had previously been shown to disrupt fiber formation,[30] the DMSO content was increased, from 25% (v/v) to 50% (v/v), and this coating procedure resulted in predominantly fiber-free GNR samples, as determined by UV-Vis spectroscopy (**Figure 4.2**) and TEM analysis (**Figure 4.3**). No broadening of the LSPR band was observed, and only a moderate red-shift (7-10 nm) was observed, indicative of a change in dielectric constant (**Figure 4.2**).[30] Individual shells formed by **1-3** were observed with TEM and accumulation of uranyl acetate revealed the shell thicknesses, which corresponded to the formation of a peptide amphiphile monolayer at the GNR surface (**Figure 4.3A-C**).

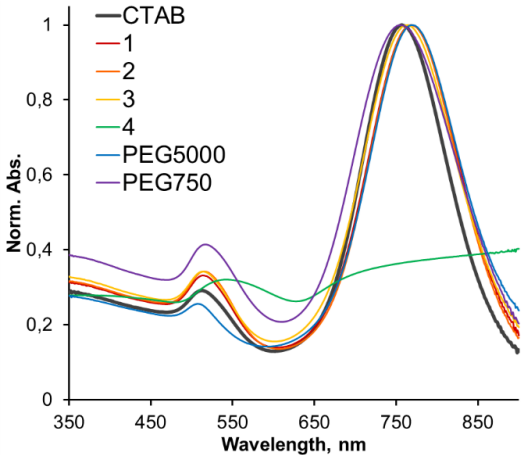

Figure 4.2. An overlay of UV-Vis spectra of GNRs with different coatings: peptide amphiphiles **1-3**, peptide **4**, and thiolated PEGs (750 and 5000 Da). Samples were prepared in PBS (pH 7.2).

Batch-to-batch variation influences the success of surface modification: some residual free fibers were observed even after increasing the DMSO content in the reaction mixture. Importantly, the initial CTAB content was found to influence fiber formation during the GNR modification protocol. Typically, CTAB is present in a high excess in GNR suspensions in order to maintain colloidal stability. When the coating with peptide amphiphiles was conducted in the presence of 10 mM CTAB (as in commercially available GNRs), the GNRs formed large aggregates visible to the naked eye within 5 mins after peptide amphiphile addition. From this, it was suspected that the cationic CTAB negatively influences the self-assembly process of the negatively charged peptide amphiphiles **1** and **3**. An imbalance between two simultaneous processes: fiber formation and Au-S bond formation, might induce the observed precipitation. Therefore, the coating procedure for GNR surface modification with peptide amphiphiles was optimized further. An additional centrifugation cycle, prior to mixing the amphiphiles and the GNRs,

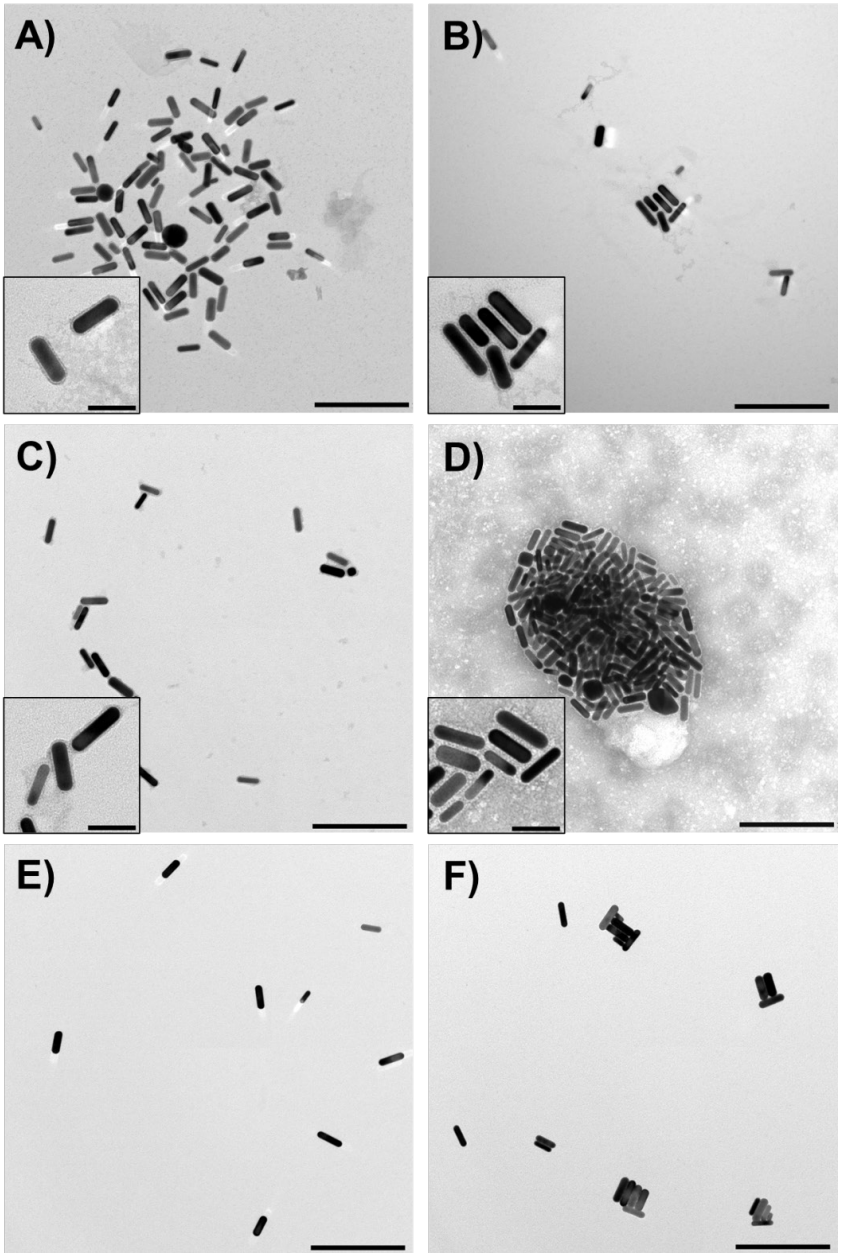

Figure 4.3. Representative TEM images of GNRs coated with: (A) **1**; (B) **2**; (C) **3**; (D) **4**; (E) PEG_{5000}; (F) PEG_{750}. Scale bars: 200 nm and 50 nm for the inserts. Samples were stained with 0.5% uranyl acetate. All samples (except **GNR@4**) were prepared in PBS (pH 7.2). Small white entities in (D) presumably derive from the peptide **4** itself, since this sample was not purified by SEC.

was added to the coating procedure to remove excess CTAB, thereby reducing GNR precipitation upon CTAB-to-peptide amphiphile exchange. GNRs, prepared according the method described in **4.5.2**, required two washing steps *via* centrifugation post-synthesis (14 000 rpm, 15 mins; the pellet was resuspended in 100 mL of water) and one extra round directly before the coating procedure. As a result, the residual CTAB concentration was sufficient to maintain colloidal stability of CTAB-protected GNRs ensuring that GNR precipitation was minimized during the peptide-amphiphile coating procedure.

Coating GNRs with molecules that did not contain an alkyl chain (molecules **4** and thiolated PEGs) was conducted in 10% (v/v) DMSO. The excess unbound molecules were removed by centrifugation, and SEC was used to exchange the buffer for PBS (pH 7.2). Coating GNRs with peptide **4** resulted in massive aggregation: UV-Vis revealed a complete loss of the LSPR band (**Figure 4.2)**. TEM imaging revealed some shell formation around the **GNR@4**, but it was not sufficient to maintain their stability in PBS (**Figure 4.3D**). The presence of the N-terminal alkyl chain indeed allowed for effective surface modification of GNRs, as reported by Schulz et al.[22] Thus, stabilization of GNRs with oligopeptides only might not be possible due to their hydrophilicity and limited penetration into the CTAB bilayer yielding incomplete coating of the GNRs.

PEGylation of GNRs resulted in a blue-shift (-1 nm) and broadening of the LSPR band for **GNR@PEG$_{750}$**, indicative of aggregation, while **GNR@PEG$_{5000}$** showed a red-shift (+11 nm) (**Figure 4.2**). This opposing behavior is explained by the change in the refractive index near the gold surface. The bandwidth was preserved in both cases, as was also observed in previous reports.[21] TEM imaging showed that **GNR@PEG$_{750}$** was present

as small compact aggregates, while **GNR@PEG$_{5000}$** consisted of well-dispersed single GNRs (**Figure 4.3E,F**). The PEG shells could not be visualized, most likely due to their low density and poor electron contrast.

All coated GNRs had a negative zeta potential in contrast to the original CTAB-stabilized GNRs, which were positively charged (-15.3 mV for **GNR@PEG$_{5000}$**, -27.3 mV for **GNR@1**, -21.1 mV for **GNR@2**, and -20.7 mV for **GNR@3** *versus* +36.6 mV for **GNR@CTAB**). This change in surface charge revealed the successful surface modification of GNRs with peptide amphiphiles.

Using the optimized coating protocol for GNRs, amphiphiles **1**-**3** proved to be effective stabilizing coatings, forming dense, well-defined shells resulting in well-dispersed single GNRs in suspension. Short peptides such as **4** are not effective as GNR stabilizers, as rapid aggregation occurred as soon as excess peptides and CTAB were removed from the GNR suspension.

4.3.3 Self-assembled monolayers formed by peptide amphiphiles on the GNR surface

TEM analysis of 21 GNRs coated with **3** showed that the shells around the **GNR@3** were not uniform in thickness (**Figure S4.1**). The shell thickness slightly differed on a rod-to-rod basis and in some cases thickness around the tips of a rod was different to the thickness around the sides (**Table S4.1**). Overall, the shell thickness distribution seemed to be curvature-independent. The average thickness was calculated to be 1.6 ± 0.3 nm both around the rod tips and around the rod sides. Interestingly, this value is lower than expected: the length of a fully-stretched molecule **3** (in a parallel β-sheet conformation and with the alkyl chain on the same axis as the peptide

backbone) was calculated to be 5.02 nm (**Scheme S4.2**). If peptide amphiphiles are situated perpendicularly to the gold surface, the expected shell thickness would be equal to the molecule length. This mismatch could be explained by several reasons. Firstly, drying effects during sample deposition on a TEM grid may cause a SAM collapse. This can implicate a change in conformation of both the peptide backbone and the alkyl chain, causing packing defects. Alternatively, it can mean that peptide amphiphiles are not positioned perpendicularly to the gold surface but at an angle. If the angle is small (<< 90°), then the peptide amphiphile shell thickness can be significantly reduced. Secondly, peptide amphiphiles consist of two segments (the alkyl chain and the peptide) with different properties and may exhibit different electron densities. The length of the C11 chain is 1.49 nm, and the rest of the molecule belongs to the peptide segment. The observed difference is most likely to be attributed to the difference in packing densities: alkyl chains undergo hydrophobic collapse and form a denser layer than the more hydrophilic peptide segments. The observed stain accumulation most likely indicates the dense part of the shell rather than the entire peptide amphiphile SAM. More information on SAM coverage densities and peptide secondary structure is needed to address this issue.

Coverage density is an important parameter defining a ligand's stabilizing capacity.[25] The coverage density of bound peptide amphiphiles was determined by UV-Vis spectroscopy as described in **Chapter 3** of this thesis.[30] For this, all three sequences were extended with a tryptophan (Trp, W) residue yielding three thiolated peptide amphiphiles **1-W**, **2-W**, and **3-W** (structures shown in **Figure S4.2**). GNRs were subsequently coated with these peptide amphiphiles. Using the extinction coefficient of Trp, $\varepsilon_{280}(W)=5600\ M^{-1}cm^{-1}$ the initial concentration of peptide amphiphiles and the amount of unbound peptide amphiphiles were determined and the number

of bound ligands was calculated. The GNRs molar concentration was calculated using $\varepsilon_{LSPR}=4.6\times10^9\ M^{-1}cm^{-1}$ and the surface area of a rod was calculated to be 2041 nm^2.[32] Unfortunately, the protocol devised for determination of peptide amphiphile coverage on the surface of spherical GNPs was not successful when applied to GNRs (**Scheme S4.1A**). A DMSO content of 50% (v/v) during the coating procedure was not sufficient to completely eliminate fiber formation and as a result the calculated coverage density for **1-W** was determined to be 10.65 peptides/nm^2, which was unrealistically high. Therefore, the maximum theoretical coverage densities d_{theor} for molecules **1-3** were calculated to determine whether the determined coverage density was theoretically possible. For this, models of fully stretched, β-structured molecules **1-3** were built using PyMol and the distances between certain atoms were determined (for details see **Scheme S4.2A**). Each molecule was simplified to a geometrical shape and, using the obtained dimensions, the volume of the molecule was calculated (**Scheme S4.2B** and **Table S4.2**). The length of a fully-stretched molecule was taken as the shell thickness, and using a diameter of the rod (14.0 nm), the volume of the shell coating was calculated (**Scheme S4.2C** and **Table S4.2**). Dividing the volume of the shell by the volume of a molecule, the following d_{theor} values were determined: 4.89 peptide/nm^2 for **1**, 4.54 peptide/nm^2 for **2** and 3.84 peptide/nm^2 for **3**. It is important to remember that these values represent a situation when the molecules are tightly packed on the gold surface with almost no free volume within the shell. These values serve as a reference, and provide a theoretical upper limit of what coverage is achievable. This calculation revealed that the determined coverage density of 10.65 peptides/nm^2 for **1-W** cannot be realistic for a SAM and is most likely is due to the presence of fibers in the sample.

The coating protocol was therefore modified once more; 1,1,1,3,3,3-hexafluoro-2-propanol (HFIP) was used as a solvent for peptide amphiphiles (**Scheme S4.1B**). HFIP was successfully used previously to disrupt the fiber formation of analogous peptide amphiphiles,[31] and to remove amyloid-like fibrils from the peptide-coated GNPs.[33] Unfortunately, this procedure also yielded high coverage densities: 7.67 peptide/nm^2 for **1-W**, 17.22 peptide/nm^2 for **2-W**, and 14.28 peptide/nm^2 for **3-W**. Again, fiber formation was suspected to be the cause of the observed behavior, which leads us to believe that trace amounts of water could sustain the presence of fibers during the HFIP washing steps. Therefore, the coating protocol was further optimized with an additional lyophilization step, introduced after the coating mixture was separated from the GNRs *via* centrifugation (**Scheme S4.1C**). This ensured that no residual water was present in the sample when the GNRs were resuspended in HFIP. UV-Vis analysis resulted in realistic coverage densities: 3.87 peptides/nm^2 for **1-W**, 3.16 peptides/nm^2 for **2-W**, and 2.62 peptides/nm^2 for **3-W**. These values are within the d_{theor} limits and are in agreement with previously reported coverage densities on GNRs coated with thiolated fatty acids, analogous to the alkyl chain our peptide amphiphiles are comprised of.[25, 26]

It should be noted that the calculated coverage densities reflected a mean ligand density throughout the whole surface area of the rod (highly curved tips and cylindrical sides) and increased in the order **GNR@3**<**GNR@2**<**GNR@1** (2.62 < 3.16 < 3.87 peptide/nm^2). It is anticipated that different coverage densities can be observed at the tips (higher) *versus* the sides (lower) of the rod, but that is yet to be determined. The order of peptide amphiphile coverage densities was explained on the basis of the molecule's geometry. Shortening the alkyl chain length from C16 to C11 directs the peptide domain closer to the gold surface. The steric bulk

of the sidechains was altered in proportion to the alkyl chain length, causing increased steric hindrance resulting in a lower coverage density for **GNR@2** in comparison to **GNR@1**. Due to the bidentate nature of **3**, a lower peptide coverage was expected.

The following parameters indicate formation of a SAM: high coverage densities, and a tight peptide packing enabling effective hydrogen bonding (hence the high level of self-assembly) within the peptide shell. It was shown that **1-3** formed SAMs on the surface of spherical GNPs (**Chapter 3** of this thesis).[30] According to Fourier-transform infrared spectroscopy (FTIR) analysis, an increased particle size resulted in a decreased surface curvature, while the content of ordered structures within the SAMs decreased. It was hypothesized that high coverage densities and the steric bulk of the peptide side chains hindered effective hydrogen bonding when the surface curvature approached a near 'flat' state. From the curvature point of view, GNRs represent a peculiar entity. A rod can be subdivided into two half-spheres with a high curvature adjacent to a cylindrical shape formed by facets. Thus, GNRs possess a combination of high and low curvature domains.

After the coating protocol was optimized to yield fiber-free samples, attenuated total reflection IR (ATR-IR) spectra of the coated GNRs were recorded to investigate peptide secondary structure. The Amide I peak (1575-1725 cm^{-1} region) describes the conformation of the peptide backbones and is a superposition of signals caused by different secondary structure types.[34, 35] An absorption band centered between 1613-1637 cm^{-1} is attributed to β-structures, a band located between 1637-1645 cm^{-1} shows the presence of unordered structures, while a band at 1645-1662 cm^{-1} is indicative of α-structures, and a band around 1662-1682 cm^{-1} reveals the

presence of turns and other structures.[34-36] The Amide I region in these recorded spectra for peptide amphiphile-coated GNRs were fitted to give a sum of these four bands (**Figure 4.4**).

As shown previously, the peptide amphiphiles used in this study form predominantly β-structures in isolation (97.7% for **1**, 85.2% for **2**, and 94.8% for **3**).[30] Indeed, no unordered structures were observed for the peptide amphiphiles in the absence of a GNR surface (**Figure 4.4A-C** and **Table S4.3**). When the peptide amphiphiles were bound to the GNR surface, all three coatings still possessed a high β-content: 58.8% for **GNR@1**, 51.8% for **GNR@2**, and 57.1% for **GNR@3** (**Table S4.3**). The tendency to adopt unordered structures was low for all three coatings (< 7%), while a significant increase in the content of turns, α-, and other structures in comparison to the free peptide amphiphiles was observed (**Table S4.3**). It should be noted that FTIR analysis of secondary structure types across the whole rod surface provides a mean distribution within the peptide shells, therefore no information was obtained about potential differences between the rod tips or sides (**Figure 4.4D-F**). The above-mentioned secondary structures were caused by packing defects that could be linked to the peptide amphiphile's composition. Molecules **2** and **3** possess a shorter (C11) alkyl chain and show a higher α-content within the shells in comparison to molecule **1**, which possesses a longer (C16) alkyl chain. Having a double alkyl chain allowed molecule **3** to increase the β-content relative to the single chain **2**. Furthermore, lower coverage densities for **2** relative to **1** suggests that the distance between the peptides might be too long to establish effective hydrogen bonding. However, the coverage densities for **2** and **3** do not correlate with the β-content: **3** showed a lower coverage density but a higher β-content. This suggests that the distance between peptide segments when **3** is attached to a surface, is sufficient to allow effective hydrogen bonding,

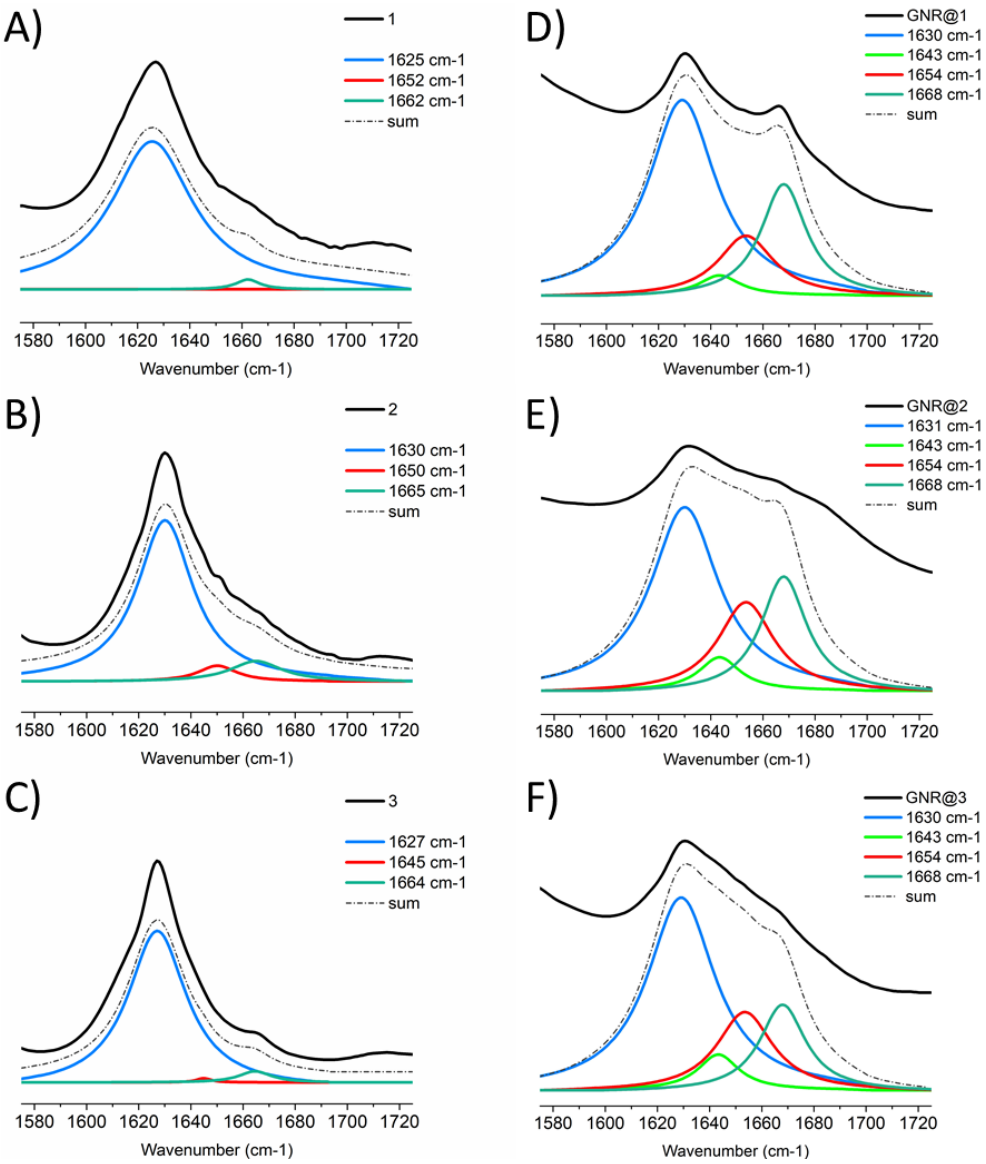

Figure 4.4. Amide I peaks were fitted to be a sum of four peaks corresponding to different secondary structure types (blue line – β-structures, green line – unordered structures, red line – α-structures, cyan line – turns). (A-C) show the Amide I fits for molecules **1-3** and were adapted from our previous work.[30] Amide I fits for GNRs coated with thiolated peptide amphiphiles are shown in (D) **1**; (E) **2**; and (F) **3**. Full ATR-IR spectra are available in the Supporting Information (**Figure S4.3**). The secondary structure distribution presented as a percentage of four different structure types is shown in **Table S4.3** (deduced from the area under the curve).

while the peptide segments of **2** are skewed by their closer proximity causing more packing defects leading to a lower β-content. In summary, a GNR coating composed of **1** or **3** is tight and restricted and therefore gives highly ordered assemblies on a surface, while **2** has more conformational freedom and packing defects, leading to less-ordered structures at the surface of a GNR.

4.3.4 Induced-aggregation behavior of peptide amphiphile-coated GNRs

Salt-induced aggregation and DTT ligand displacement assays were employed as induced-aggregation tests to investigate the ligand organization on the gold surface and the origin of the observed stability (**Chapter 3** of this thesis).[30] Furthermore, these assays probe colloidal stability of coated GNRs under extreme conditions using UV-Vis spectroscopy. For comparison to state of the art, peptide amphiphile protective coatings for GNRs were compared to PEG coatings.

NaCl induces GNR aggregation by screening surface charges, resulting in the nanoparticles reaching their isoelectric point. As a result, interparticle electrostatic repulsion is minimized, and the aggregated nanoparticles precipitate from suspension. In this assay, surface-modified GNRs were exposed to NaCl at concentrations of 150 mM, 500 mM, 1.5 M, and 3.0 M respectively for 15 min and UV-Vis spectra were recorded (**Figure S4.4**). The aggregation state was determined by the absorbance of the LSPR band: the decrease in the optical density at the LSPR wavelength (OD_{LSPR}) relative to the OD_{LSPR} of the sample in 0 mM NaCl indicated aggregation (equation is shown in **Figure 4.5B**).[30] Severe aggregation was considered to occur if the value of normalized OD_{LSPR} was below 0.5. GNRs coated with the single

chain amphiphiles **1** and **2** showed rapid (*i.e.* within 15 mins) aggregation when the NaCl concentration was increased from 150 to 500 mM, while GNRs coated with the double-chain amphiphile **3** were insensitive to high NaCl concentrations, even up to 3.0 M. PEGylated GNRs did not exhibit severe aggregation, but a 10-15% decrease in absorbance relative to the 0 M NaCl state indicated that PEGylated GNRs are more sensitive to charge screening than **GNR@3**. Rapid NaCl-induced aggregation of **GNR@1** and **GNR@2** most likely arises from their chemical structure, resulting in a different charge distribution on the surface of these coated GNRs in comparison to **3**. Interestingly, the zeta potential values were similar for all three peptide amphiphile coated GNRs (deviation ± 5 mV), and therefore cannot be used as a predictor of colloidal stability. These results suggest that the charge distribution, as well as the peptide chain conformation (its secondary structure) and coverage densities are dictated by the alkyl chain parameters (number of chains and their length). Presumably, the C-terminal glutamate residues of **3** are more exposed to the environment when coupled to a surface in comparison to **1** or **2** and therefore provide a stabilizing effect. It should be noted, that upon removal of NaCl (by means of centrifugation) the peptide amphiphile-stabilized GNRs regained their non-aggregated state, which means that the observed aggregation was reversible and should be considered agglomeration.

Next, the DTT competition assay was conducted to probe the accessibility of the gold surface and the stability of the Au-S bond: if ligands are displaced with DTT, GNRs aggregate. For this assay, coated GNRs were exposed to 1 M DTT and a UV-Vis spectrum was recorded every 5 mins (**Figure S4.5**). The aggregation factor (AF)[30, 37] was calculated as the ratio between the optical density at 610 nm (OD_{610}), a peak indicative of aggregation, and the

OD_{LSPR}. This value is then normalized to the initial value: AF_0 (equation is shown in **Figure 4.5C**).

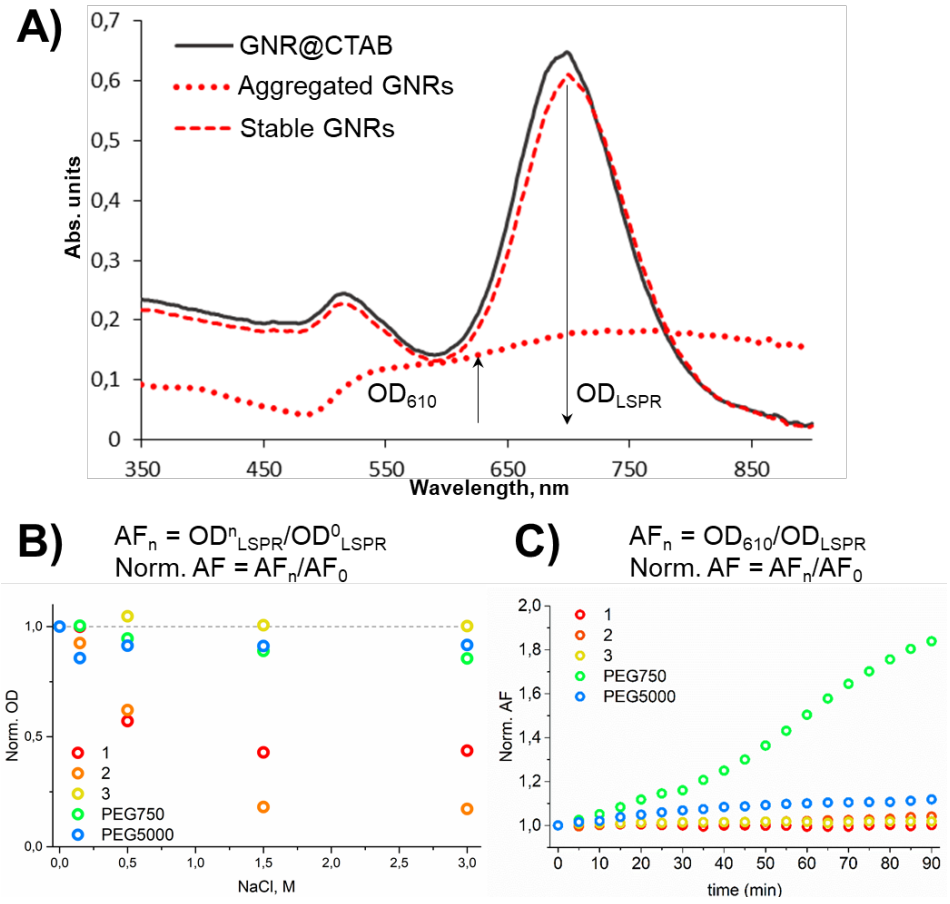

Figure 4.5. Aggregation behavior of coated GNRs was monitored as shown in schematic (A): upon aggregation the LSPR band is lost; its intensity significantly decreases in respect to the absorbance at 610 nm. Aggregation factors (AF) were calculated according to the equations and normalized to the value at t = 0 min. (B) Normalized AF calculated for coated GNRs in the presence of high salt concentrations; (C) Normalized AF calculated for coated GNRs in the presence of 1 M DTT. UV-Vis spectra the calculations were based on can be found in **Figure S4.4** and **Figure S4.5**.

From the normalized AF plot (**Figure 4.5C**) it was obvious that all three thiolated peptide amphiphiles protected and insulated the GNR surface by

forming an impenetrable monolayer. This was attributed to the high coverage densities provided by the alkyl chains, as well as to the presence of the hydrophobic environment created by the alkyl chains. Water and polar molecules dissolved in it cannot penetrate the hydrophobic barrier and are depleted from the gold surface. In contrast, the colloidal stability of PEGylated GNRs was shown to be strongly correlated to the molecular weight of the PEG. While **GNR@PEG$_{750}$** aggregated rapidly, **GNR@PEG$_{5000}$** did not exhibit signs of aggregation. GNR stabilization with PEG is based on a steric stabilization effect: the long polymer chain wraps around the surface providing good coverage and shielding. As a result, longer PEGs provide better coverage of the gold surface, while shorter PEG cannot not obtain a proper conformation to do so.[21]

Based on the combined results from both tests (**Figure 4.5B,C**), GNR coating with peptide amphiphile **3** outperformed thio-PEG$_{5000}$. **GNR@3** was completely insensitive to the surface charge screening, and did not dissociate from the gold surface upon addition of a competing thiolated ligand. At the same time the thiolated PEG$_{5000}$ coating, a molecule that greatly exceeds the length of **3**, did show some aggregation in both assays. The superior stability of **3** as a GNR coating was a result of the two alkyl tails providing an increased hydrophobic bulk and four Glu residues *versus* three residues in **1** and **2**. The contribution of the double chain was reflected in a different peptide chain arrangement allowing for the display of more charges on the shell surface than in the case of **1** or **2**. The bidentate nature of **3** is also beneficial because such coordination was proven to be more stable compared to monodentate counterparts.[37]

4.3.5 Peptide amphiphiles provide stabilizing coatings regardless of the GNR aspect ratio

GNR dimensions and aspect ratios (a.r.) can be tuned to provide desired optical properties,[4] and we validated whether thiolated peptide amphiphiles are able to stabilize GNRs with different dimensions. For this, GNRs with the a.r. range of 2.9-4.1 were used (**Table 4.1**). As expected, coating of GNRs with the more hydrophobic amphiphiles **1** and **3** resulted in shell formation alongside fiber formation: apparent from UV-Vis spectra and TEM images, while coating with **2** was not accompanied by fiber formation (**Figure 4.6A,B**). Well-defined shells for **1**, **2**, and **3** corresponding to a ligand monolayer were visible as well. Interestingly, the zeta potential values were within the -20 to -30 mV range, regardless of the GNR a.r. or applied peptide amphiphile coating.

Table 4.1. Size characteristic of GNRs used in this study.

Sample	Length, nm (± SD*)	Width, nm (± SD)	A.r.
GNR	46.4 ± 8.3	14.0 ± 2.9	3.3
s-GNR**	44.0 ± 4.0	14.8 ± 1.9	2.9
l-GNR***	49.0 ± 9.1	12.0 ± 2.6	4.1

Average size of GNRs was determined using TEM. *- SD = standard deviation. **- short GNRs (**s-GNR**) were synthesized according to the method described in **4.5.2**, but had different dimensions compared to the **GNR** sample (within batch-to-batch variations). ***- long GNRs (**l-GNR**) were purchased from Sigma-Aldrich.

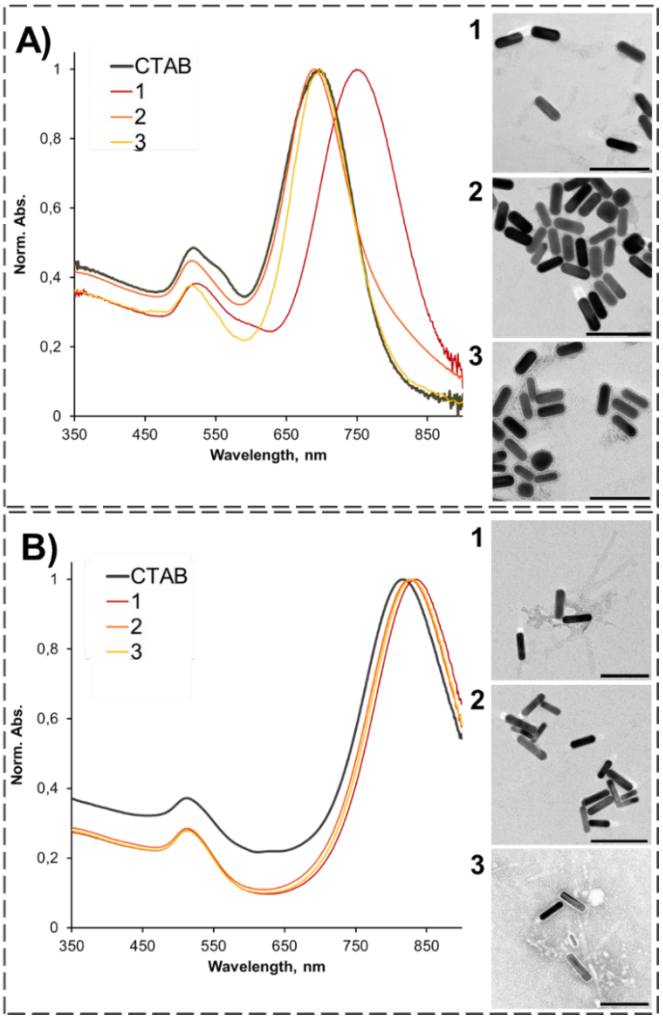

Figure 4.6. Sample characterization (UV-Vis spectroscopy on the left and TEM imaging on the right) for peptide amphiphile-coated GNRs with different a.r.: (panel A) **s-GNRs** and (panel B) **l-GNRs** Samples were prepared in PBS (pH 7.2). The non-optimized protocol was used to fabricate the samples; hence peptide amphiphile fibers are present. In the case of **s-GNR@1**, a significant red-shift was observed due to the presence of associated fibers triggering interparticle interactions. Scale bar is 100 nm. Negative staining (0.5% uranyl acetate) was used.

4.3.6 Positively charged peptide amphiphile-stabilized GNRs

Peptide amphiphiles can be designed to carry either net negative (as for molecules **1-3**) or positive charge.[38] Two thiolated peptide amphiphiles dubbed **1-K** and **2-K**, in which Glu residues were replaced by Lys residues, were synthesized (sequences are shown in **Figure S4.6**). Due to the opposite charge, the coating procedure had to be altered. As a result, fiber formation was not observed, possibly due to the electrostatic repulsion between the positively charged CTAB and lysine-rich peptide amphiphiles. Furthermore, the coating procedure was conducted in 10% DMSO (aq., v/v) and extended to 16 hours instead of 1 hour, and SEC purification was done with water as the eluent. UV-Vis spectroscopy revealed a small red-shift (+7 nm) for **GNR@1-K** and aggregation did not occur. Although a larger red-shift (+16 nm) was observed for **GNR@2-K**, TEM imaging revealed no aggregation, and no peptide amphiphile fibers, hence this red-shift cannot arise from association with peptide amphiphile fibers (**Figure 4.7**). The shifts were explained by a change in refractive index at the GNR surface upon CTAB exchange.[18] The zeta potential was positive for both coated samples (+23.6 mV for **GNR@1-K**, +18.7 mV for **GNR@2-K** *versus* +36.6 mV for **GNR@CTAB**). The NaCl-aggregation assay was applied to the positively charged **GNR@1-K** and **GNR@2-K**. The samples were exposed to increasing NaCl concentrations for 15 min and the OD_{LSPR} was monitored. (**Figure 4.7C** and **Figure S4.6**). GNRs coated with positively charged **1-K** and **2-K** already aggregated at 50 mM NaCl, when all surface charges were screened and the isoelectric point was reached. This implies that **GNR@1-K** and **GNR@2-K** cannot be used in biologically relevant conditions.

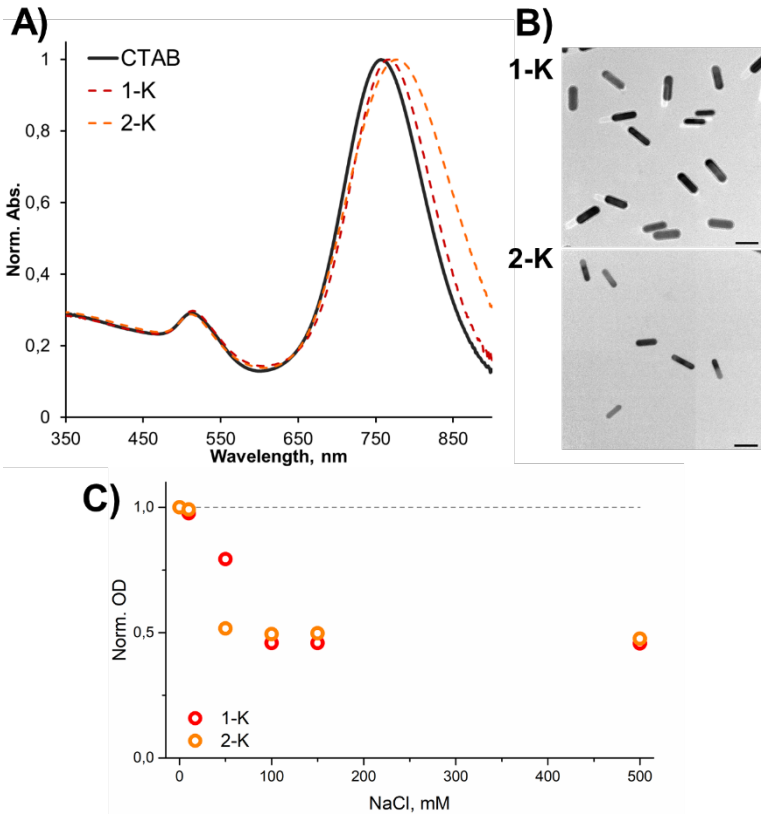

Figure 4.7. Characterization of GNRs coated with positively charged **1-K** and **2-K**: (A) UV-Vis spectroscopy and (B) TEM imaging. Samples were prepared in MQ water. Scale bar is 50 nm. Negative staining (0.5% uranyl acetate) was used. (C) Normalized AF calculated for coated GNRs in the presence of high salt concentrations. Aggregation factor values (AF) were calculated according to the equations shown in **Figure 4.5B** and were normalized to the value at t = 0 min. UV-Vis spectra the calculations were based on can be found in **Figure S4.6**.

4.4 Conclusions

Thiolated peptide amphiphiles were evaluated for their ability to form a protective coating at the GNR surface. Peptides that did not contain an alkyl chain failed to stabilize GNRs. However, it was proven that both negatively charged amphiphiles **1-3** and positively charged **1-K** and **2-K** are capable of displacing CTAB from the GNR surface and stabilize GNRs irrespective of their aspect ratio. The negatively charged peptide amphiphile-stabilized GNRs possess long-term stability under physiologically relevant conditions. Thiolated, negatively-charged, peptide amphiphiles provide greater stability compared to commonly used thiolated PEG of the same molecule length. Furthermore, thiolated peptide amphiphiles provide a much thinner coating with equal stabilizing capacity in comparison to long thiolated PEG. Peptide amphiphiles also offer relatively easy pathways for modification with ligands, while modification of long thiolated PEGs is not trivial. Moreover, PEGs were reported to induce specific immune responses,[39] while peptide amphiphiles are not recognized by the immune system.[40]

The stabilizing effect of the amphiphiles was attributed to the presence of an alkyl chain and to the formation a self-assembled monolayer (SAM) bound to the GNR surface. Both the number and length of the alkyl chain proved to be important factors influencing the peptide amphiphile self-assembly on the surface. Peptide amphiphiles with a single alkyl chain **1** (C16 length) and **2** (C11 length) showed higher coverage densities with respect to the bidentate peptide amphiphile **3** (double C11). ATR-IR analysis of the secondary structure of the GNR-bound peptide amphiphiles revealed that all three peptide amphiphiles formed ordered assemblies on the GNR surface in comparison to peptide amphiphile **2**, with a slightly lower β-content (<7%). At

NaCl concentrations exceeding biologically relevant levels, GNRs coated with the single chain peptide amphiphiles **1** and **2** showed that the surface charge of such GNRs is more easily screened than in the case of GNRs coated with the double chain **3**. These findings suggest that despite similar self-assembly behavior and high coverage densities, there is a delicate difference in the peptide domain assembly at the GNR surface. According to the induced aggregation tests, peptide amphiphile **3** was considered to be the best stabilizer for GNRs as **GNR@3** was stable at high NaCl and DTT concentration.

Coatings based on peptide amphiphiles **1-3** were previously applied to stabilize spherical GNPs (**Chapter 3** of this thesis).[30] Similarly to the behavior of **3** on the surface of 20 and 40 nm GNPs, **GNR@3** showed superior stability even in 3.0 M NaCl (**Figure 4.5B**). Both single chain peptide amphiphiles **1** and **2** could not prevent reversible nanoparticle agglomeration at 500 mM NaCl. GNPs and GNRs possess different kinds of curvature: GNRs have both spherical (tips) and cylindrical (sides) parts. This seems to suggest that the charge distribution on the cylindrical surface did not differ significantly from the charge distribution on the spherical surface.

Obtained guidelines on the coating protocol and data on peptide amphiphile-stabilized GNRs encourage the use of these nanoparticles in biological applications *in vitro* and *in vivo*. Peptide amphiphile-stabilized GNRs equipped with specific ligands can be used in label-free biosensing, as well as in imaging, and as a delivery platform. **Chapter 5** of this thesis will focus on employing peptide amphiphile-stabilized GNPs and GNRs in vaccine development.

4.5 Experimental section

4.5.1 Materials

All chemicals were purchased from Sigma-Aldrich unless stated otherwise. For GNR and GNP synthesis, the purity of CTAB and the composition of the gold salt are critical for reliable particle formation. CTAB (≥ 99%, H6269) and $HAuCl_4 \times 3\ H_2O$ (49% Au basis, G4022) were purchased from Sigma-Aldrich. Silver nitrate (99,9999%, 4500.1) and Oxyma Pure were purchased from Carl Roth GmbH. TFA, piperidine, DMF, DCM, methanol, and acetonitrile were purchased from Biosolve. Thiolated PEGs ($HS\text{-}PEG\text{-}OCH_3$ with average MW of 750 Da and 5000 Da) were supplied by Rapp Polymere GmBH. TEM grids (Formvar/Carbon, 200 mesh, on copper support) were purchased from Electron Microscopy Sciences. Gold nanorods (GNRs) with an a.r. of 4.1 were purchased from Sigma-Aldrich (LSPR at 810 nm).

4.5.2 GNRs synthesis

Gold nanorods (GNRs) were synthesized in the presence of CTAB in the two-step process commonly described as seed-mediated approach.[3] Briefly, 2-3 nm seeds were prepared by mixing the following solution: CTAB (5 mL, 0.20 M), $HAuCl_4$ (5 mL, 0.50 mM) with ice-cold $NaBH_4$ (0.60 mL, 10 mM) added under intense stirring at room temperature.[32] After 2 mins of vigorous stirring, the solution was left undisturbed at room temperature for 2 hours. For the overgrowth, solutions of $HAuCl_4$ (50 mL, 1.0 mM) and $AgNO_3$ (200 µL,100 mM) were gently mixed with CTAB (50 mL, 0.20 M) at 25 ºC. The amount of silver added is the major determinant for the aspect ratio (a.r.) of the resulting GNRs. After 2 min of stirring, ascorbic acid (550 µL, 100 mM) was added. The growth solution underwent a color change from dark yellow

to colorless due to reduction of gold. Next, 120 µL of the seed solution was added to the growth solution under vigorous stirring at room temperature. After 6 hours the rods were washed with MilliQ twice (2 × 100 mL) by means of centrifugation to remove the CTAB excess. Average dimensions were found to be 46.4 by 14.0 nm as determined by TEM.

Due to the high sensitivity of this synthetic procedure to the quality of some reagents, slight alterations to the protocol may be needed. Increasing the volume of 100 mM $AgNO_3$ to 400 µL may be necessary to make GNRs with an a.r. of 3.0. If shape control is lost and non-rodlike particles are formed instead of GNRs, it is recommended to adjust the ratio between $HAuCl_4$ and ascorbic acid.

4.5.3 Peptide and peptide amphiphile synthesis

All peptide amphiphile and peptide sequences were synthesized by solid-phase peptide synthesis using standard Fmoc-chemistry protocols (9-fluorenylmethyloxycarbonyl-protected amino acids were used to propagate the peptide chain). The synthesis was performed on an automated microwave peptide synthesizer Liberty Blue (CEM) using standard settings. 5 equivalents (relative to the resin loading) of Fmoc-protected amino acids were used to propagate the peptide chain. 20% piperidine in dimethylformamide (DMF) was used as the deprotection agent (90 °C, 60 secs) and N,N'-diisoprorylcarbodiimide (DIC)/OxymaPure were employed as the activator/activator base pair (5 equivalents relative to the resin loading, 95 °C, 4 mins). The sequences were synthesized on a high-loading Wang resin (**1-4**, **1-W**, **2-W**, **3-W**) or a high-loading Rink Amide resin (**1-K** and **2-K**), yielding either a C-terminal acid (**1-4**) or an amide (**1-K** and **2-K**) at 0.1 mmol scale. Used resin loadings were within the range of 0.5-0.8 mmol/g. The alkylation was performed using Liberty Blue *via* an on-resin coupling of

the corresponding chain to the terminal amine of the corresponding peptide (the same protocol as for amino acids). The terminal thiol of acyl chains was blocked with 2,2′-Dithiobis(5-nitropyridine) (DTNP, 1 eq. in DMF, 3 hours). Peptide **4** was not alkylated, thus preserving a free amine at the N-terminus. All the molecules were cleaved from the resin using a trifluoroacetic acid (TFA) cocktail: 1.5% deionized water, 2.5% triisopropylsilane (TIS), and in the case of **4**, 2.5% 3,4-ethylenedioxythiophene (EDOT) was added. The crude peptide amphiphiles were precipitated into cold diethyl ether, pelleted by centrifugation, redissolved in water, and lyophilized prior to purification.

4.5.4 Peptide amphiphile purification

A Shimadzu HPLC system equipped with two LC-20AR pumps, an SPD-20A UV-Vis detector and a Phenomenex Kinetex EVO C18 column (21.2 by 150 mm) was used to perform HPLC purification of the peptidic molecules. The mobile phases were water and acetonitrile, containing either 0.1% NH_3 (for **1-3**) or 0.1% TFA (for **4**, **1-K**, and **2-K**). Acetonitrile gradients were run over 25 min with a flow rate of 12 mL/min: **1-3** were purified on a 5-55% gradient of acetonitrile; **1-K** – 20-100%; and **2-K** – 15-75%. Prior to purification of **1-3**, the protecting TNP group was removed by Tris(2-carboxyethyl)phosphine hydrochloride (TCEP, added in excess, 30 mins incubation). The purity of the compounds was assessed using LC-MS (**Figures S4.7-15**). All purified molecules were lyophilized and stored at -20 °C until needed.

4.5.5 Coating GNRs with thiolated peptide amphiphiles

GNRs were coated using a ligand exchange approach. The ligand (*i.e.* peptide amphiphiles) was dissolved in DMSO and added to a stirred GNR suspension. The ligand excess was at least 100 000-fold (molar) relative to

the GNR concentration obtained using extinction coefficients for GNRs with different a.r. published by Orendorff *et al*.[32] In other words, for every mL of GNR suspension with the optical density of absorbance maximum (OD_{LSPR}) of 1, at least 0.05 mg of a peptide amphiphile was added. The two components were mixed in such a ratio (v/v) to assure that the final concentration of DMSO in the mixture was 50% (v/v) for **GNR@1**, **GNR@2**, and **GNR@3**, and 10% (v/v) for **GNR@4**, **GNR@1-K**, and **GNR@2-K**. After the incubation (1 hour for **1-3**; 16 hours for **1-K** and **2-K**) the samples were centrifuged (Eppendorf Centrifuge 5425, 14 000 rpm, 15 mins), the supernatants were discarded and replaced with 25% DMSO in water (**GNR@1**, **GNR@2**, and **GNR@3**) or 5% DMSO in water (**GNR@4**, **GNR@1-K**, and **GNR@2-K**). **GNR@4**, **GNR@1-K**, and **GNR@2-K** were directly loaded on a size exclusion chromatography column (SEC, NAP-25 columns, GE Healthcare) to remove any remaining free ligand and exchange for phosphate buffered saline (PBS). The **GNR@1**, **GNR@2**, and **GNR@3** samples were incubated in DMSO, 25% (v/v) overnight to dissolve unbound peptide amphiphiles. After centrifugation, supernatants were discarded and the GNRs were resuspended in 5% DMSO (v/v) the same SEC purification was performed. If fiber formation by **1** and **3** occurred, the samples were lyophilized, resuspended in pure DMSO, incubated overnight and SEC-purified as described above.

4.5.6 PEGylation of GNRs

Thiolated PEGs were dissolved in DMSO (10 mg/mL). The added PEG excess was at least 100 000-fold relative to GNR molar concentration. For every mL of a GNR suspension with the OD_{LSPR} of 1 at least 0.2 mg of PEG was added. The PEG solution and GNR suspension were mixed resulting in a 10% (v/v) final concentration of DMSO. GNRs were PEGylated in 10% DMSO (v/v) mixtures overnight and PEG was removed *via* centrifugation

(14 000 rpm, 15 mins). GNRs were resuspended in MQ and directly purified by means of SEC (NAP-25 column, GE Healthcare) with PBS as the eluent according to the manufacturer's manual.

4.5.7 UV-Vis spectroscopy

Spectra were recorded using a Cary 300 UV-Vis spectrophotometer (Agilent). Samples were placed in 1 mm quartz cuvettes and spectra were recorded between 900-350 nm unless otherwise stated. Samples were diluted with either MQ water or PBS as appropriate to provide a maximum absorbance in the range of 0.6-1.0. All spectra were normalized to a maximum absorbance of 1.0, except for the induced aggregation experiments where spectra were not normalized and aggregation factors were calculated as described in **4.5.12** and **4.5.13**. To calculate peptide amphiphile and GNR concentration, Lambert-Beer law was used (equation 1):

$$A = \varepsilon \cdot l \cdot c \cdot N, \quad (1)$$

where A is absorption, ε is extinction coefficient (in $M^{-1}cm^{-1}$), l is the optical path length (l = 1 mm), c is molar concentration (in M), and N is the dilution factor. For GNRs with an a.r. of 3.3, $\varepsilon_{LSPR}(GNR)=4.6\times10^9$ $M^{-1}cm^{-1}$ was used.[32] For tryptophan absorbance $\varepsilon_{280}(W)=5600$ $M^{-1}cm^{-1}$ was used.

4.5.8 Transmission electron microscopy

Grid preparation for transmission electron microscopy (TEM) measurements involved the following steps: a 10 µL GNR sample droplet was placed on a continuous carbon grid (200 mesh copper support) and left undisturbed for 10 mins. The excess sample was removed by manually blotting with a fibreless paper tissue (Kimtech Science). A water droplet (10 µL) was put on

the grid to wash off the unbound sample and blotted once again right away. Uranyl acetate staining (0.5% w/v, 10 µL, t = 10 secs) was applied, followed immediately by blotting. Images were acquired on a JEM1400 Plus (JEOL) transmission electron microscope operated at 80 kV and equipped with a CCD camera.

4.5.9 Zeta potential measurements

A Zetasizer Nano-7 S (Malvern Instruments) equipped with a 633 nm laser wavelength and a 173° fixed scattering angle was used to perform zeta potential measurements. Samples in PBS were diluted 10 times with deionized water to obtain a salt concentration below 20 mM. Sample aliquots of 1 mL were placed in a universal dip cuvette and the zeta potential was calculated from an average of three measurements.

4.5.10 Coverage density measurements

Coverage densities were determined through the unbound ligand content.[41] The three thiolated peptide amphiphiles were extended with a Tyr coupled *via* a glycine spacer to yield **1-W**, **2-W**, **3-W** (**Figure S4.2**). These three molecules were used to coat GNRs in an altered setup: three different protocols were devised (workflows schematically shown in **Scheme S4.1**). The ratio between GNR and peptide amphiphile concentrations was preserved (see, **4.5.5**). Lambert-Beer was used to determine peptide and GNR concentrations (equation 1: $\varepsilon_{280}(W)=5600\ M^{-1}cm^{-1}$; $\varepsilon_{LSPR}(GNR)=4.6\times10^{9}\ M^{-1}cm^{-1}$).

Protocol #1 (**Scheme S4.1A**). Tryptophan-tagged peptide amphiphiles **1-W**, **2-W**, and **3-W** were dissolved in DMSO and mixed with CTAB-protected GNRs in the same molar ratio as described above (**4.5.5**), yielding a final

DMSO concentration of 50% (v/v). After a 1-hour incubation, the supernatant of the first centrifugation cycle was collected and combined with the supernatant of the following wash with 25% DMSO (v/v). The supernatants were analyzed by UV-Vis with absorbance at 280 nm. As the concentration of **1-W**, **2-W**, and **3-W** added to the GNR suspension was known, the concentration of unbound ligands in the combined supernatants was determined using UV-Vis, the number of bound ligands was calculated. The number of ligands per particle was calculated by dividing the concentration of the bound ligands by the molar concentration of original GNRs (calculated as described elsewhere).[32] The coverage density expressed in peptide/nm^2 was derived from the average surface area of a rod.

Protocol #2 (**Scheme S4.1B**). Tryptophan-tagged molecules **1-W**, **2-W**, and **3-W** were dissolved in 1,1,1,3,3,3-hexafluoro-2-propanol (HFIP) and mixed with CTAB-protected GNRs in the same molar ratio as described above (**4.5.5**), but yielding a final HFIP concentration of 33% (v/v). After a 1-hour incubation, the supernatant of the first centrifugation cycle was collected and combined with the supernatant of the following wash with HFIP. The supernatants were analyzed using UV-Vis and absorbance at 280 nm was determined. As the concentration of **1-W**, **2-W**, and **3-W** added to the GNR suspension was known, the concentration of unbound ligands in the combined supernatants was determined using UV-Vis, and it was possible to deduce the amount of bound ligands. The number of ligands per particle was calculated by dividing the concentration of the bound ligands by the molar concentration of original GNRs (calculated as described elsewhere).[32] The coverage density expressed in peptide/nm^2 was derived from the average surface area of a rod.

Protocol #3 (**Scheme S4.1C**). Tryptophan-tagged molecules **1-W**, **2-W**, and **3-W** were dissolved in HFIP and mixed with CTAB-protected GNRs in the

same molar ratio as described above (**4.5.5**), but yielding a final HFIP concentration of 33% (v/v). After a 1-hour incubation, the supernatant of the first centrifugation cycle was collected. The GNR pellets were resuspended in water and lyophilized. Next, GNRs were resuspended in HFIP and were pelleted again. The supernatants were analyzed using UV-Vis and absorbance at 280 nm was determined. Since the concentration of **1-W**, **2-W**, and **3-W** added to the GNR suspension was known, the concentration of the unbound ligands in the combined supernatants was determined using UV-Vis, and the number of bound ligands was calculated. Next, the number of ligands per particle was calculated by dividing the concentration of bound ligands by the molar concentration of original GNRs (calculated as described elsewhere).[32] The coverage density expressed in peptide/nm^2 was derived from the average surface area of a rod.

4.5.11 Infra-red spectroscopy measurements

Attenuated total reflection-infrared (ATR-IR) spectra were recorded on an Excalibur FTS 4000 setup equipped with a “golden gate” accessory. Samples were analyzed in the solid state (both thiolated peptide amphiphiles and coated GNRs). A lyophilized powder was placed on top of the crystal and spectra were recorded (512 scans at 2 cm^{-1} aperture). Deconvolution and fitting of the Amide I peaks to the Lorenz function were performed using Origin Pro. Surface areas under the individual peaks were taken to determine the distribution of different peptide secondary structure types.

4.5.12 Stability to electrolyte-induced aggregation

GNRs coated with **1-3**, thio-PEG$_{5000}$, and thio-PEG$_{750}$ were mixed with a 4.5 M NaCl solution to yield samples with the following final concentrations of salt: 150 mM, 500 mM, 1.5 M and 3.0 M. The GNR concentration

remained constant (OD_{LSPR} ~ 0.2-0.4) while only the salt concentration was varied. A spectrum from 500–800 nm was recorded using an Infinite M1000 plate-reader (Tecan). The optical densities at the peak maximum of the LSPR (OD_{LSPR}) of each sample were compared to that of a GNR suspension with no salt added (0 mM NaCl). When GNRs aggregate, they exhibit a red-shift and often a broadening of the plasmon band. The OD of the samples with increasing amounts of NaCl were monitored and a decrease in the OD_{LSPR} value indicated aggregation.

4.5.13 Stability to DTT-competition induced aggregation

A DL-Dithiothreitol (DTT) competition assay was used to assess permeability of the peptide amphiphile shells formed around the GNRs. The protocol used in this study was a modification of that published by the Mattoussi group.[37] Briefly, 4 M DTT, deionized water and the coated GNRs were mixed in a proportion to set the final concentration of DTT to 1 M. The OD_{LSPR} value was monitored by UV-Vis for 90 mins with a 5 min interval between the data points to assess the aggregation state. The OD_{LSPR} at the 0 min time point was maintained within a range of 0.5-0.9 for all GNR samples. The ratio between the OD at 610 nm and OD_{LSPR} gave rise to the aggregation factor (AF), which was normalized to the value at t = 0 min.

4.6 References

1. Lohse, S. E.; Murphy, C. J., The Quest for Shape Control: A History of Gold Nanorod Synthesis. *Chem Mater* **2013,** *25* (8), 1250-1261.

2. Link, S.; Burda, C.; Mohamed, M. B.; Nikoobakht, B.; El-Sayed, M. A., Laser photothermal melting and fragmentation of gold nanorods: Energy and laser pulse-width dependence. *J Phys Chem A* **1999,** *103* (9), 1165-1170.

3. Nikoobakht, B.; El-Sayed, M. A., Preparation and growth mechanism of gold nanorods (NRs) using seed-mediated growth method. *Chem Mater* **2003,** *15* (10), 1957-1962.

4. Gonzalez-Rubio, G.; Kumar, V.; Llombart, P.; Diaz-Nunez, P.; Bladt, E.; Altantzis, T.; Bals, S.; Pena-Rodriguez, O.; Noya, E. G.; MacDowell, L. G.; Guerrero-Martinez, A.; Liz-Marzan, L. M., Disconnecting Symmetry Breaking from Seeded Growth for the Reproducible Synthesis of High Quality Gold Nanorods. *ACS Nano* **2019,** *13* (4), 4424-4435.

5. Wang, H. F.; Huff, T. B.; Zweifel, D. A.; He, W.; Low, P. S.; Wei, A.; Cheng, J. X., In vitro and in vivo two-photon luminescence imaging of single gold nanorods. *P Natl Acad Sci USA* **2005,** *102* (44), 15752-15756.

6. Durr, N. J.; Larson, T.; Smith, D. K.; Korgel, B. A.; Sokolov, K.; Ben-Yakar, A., Two-photon luminescence imaging of cancer cells using molecularly targeted gold nanorods. *Nano Letters* **2007,** *7* (4), 941-945.

7. Tong, L.; Wei, Q. S.; Wei, A.; Cheng, J. X., Gold Nanorods as Contrast Agents for Biological Imaging: Optical Properties, Surface Conjugation and Photothermal Effects. *Photochem Photobiol* **2009,** *85* (1), 21-32.

8. Zhang, W. C.; Caldarola, M.; Lu, X. X.; Orrit, M., Plasmonic Enhancement of Two-Photon-Excited Luminescence of Single Quantum Dots by Individual Gold Nanorods. *ACS Photonics* **2018,** *5* (7), 2960-2968.

9. van den Broek, B.; Ashcroft, B.; Oosterkamp, T. H.; van Noort, J., Parallel Nanometric 3D Tracking of Intracellular Gold Nanorods Using Multifocal Two-Photon Microscopy. *Nano Letters* **2013,** *13* (3), 980-986.

10. Knights, O. B.; Ye, S. J.; Ingram, N.; Freear, S.; McLaughlan, J. R., Optimising gold nanorods for photoacoustic imaging in vitro. *Nanoscale Adv* **2019,** *1* (4), 1472-1481.

11. Xu, K. Y.; Shi, J. W.; Pourmand, A.; Udayakumar, T. S.; Dogan, N.; Zhao, W. Z.; Pollack, A.; Yang, Y. D., Plasmonic Optical Imaging of Gold Nanorods Localization in Small Animals. *Sci Rep-Uk* **2018,** *8*: e9342.

12. Bhamidipati, M.; Fabris, L., Multiparametric Assessment of Gold Nanoparticle Cytotoxicity in Cancerous and Healthy Cells: The Role of Size, Shape, and Surface Chemistry. *Bioconjugate Chem* **2017,** *28* (2), 449-460.

13. Yelin, D.; Oron, D.; Thiberge, S.; Moses, E.; Silberberg, Y., Multiphoton plasmon-resonance microscopy. *Opt Express* **2003,** *11* (12), 1385-1391.

14. Sonnichsen, C.; Alivisatos, A. P., Gold nanorods as novel nonbleaching plasmon-based orientation sensors for polarized single-particle microscopy. *Nano Letters* **2005,** *5* (2), 301-304.

15. Abadeer, N. S.; Murphy, C. J., Recent Progress in Cancer Thermal Therapy Using Gold Nanoparticles. *J Phys Chem C* **2016,** *120* (9), 4691-4716.

16. Wu, Y.; Ali, M. R. K.; Dong, B.; Han, T. G.; Chen, K. C.; Chen, J.; Tang, Y.; Fang, N.; Wang, F. J.; El-Sayed, M. A., Gold Nanorod Photothermal Therapy Alters Cell Junctions and Actin Network in Inhibiting Cancer Cell Collective Migration. *ACS Nano* **2018,** *12* (9), 9279-9290.

17. Cao, J.; Sun, T.; Grattan, K. T. V., Gold nanorod-based localized surface plasmon resonance biosensors: A review. *Sensor Actuat B-Chem* **2014,** *195*, 332-351.

18. Paulo, P. M. R.; Zijlstra, P.; Orrit, M.; Garcia-Fernandez, E.; Pace, T. C. S.; Viana, A. S.; Costa, S. M. B., Tip-Specific Functionalization of Gold Nanorods for Plasmonic Biosensing: Effect of Linker Chain Length. *Langmuir* **2017,** *33* (26), 6503-6510.

19. Scarabelli, L.; Sanchez-Iglesias, A.; Perez-Juste, J.; Liz-Marzan, L. M., A "Tips and Tricks" Practical Guide to the Synthesis of Gold Nanorods. *J Phys Chem Lett* **2015,** *6* (21), 4270-4279.

20. Ye, X. C.; Gao, Y. Z.; Chen, J.; Reifsnyder, D. C.; Zheng, C.; Murray, C. B., Seeded Growth of Monodisperse Gold Nanorods Using Bromide-Free Surfactant Mixtures. *Nano Letters* **2013,** *13* (5), 2163-2171.

21. Bogliotti, N.; Oberleitner, B.; Di-Cicco, A.; Schmidt, F.; Florent, J. C.; Semetey, V., Optimizing the formation of biocompatible gold nanorods for cancer research: Functionalization, stabilization and purification. *J Colloid Interf Sci* **2011,** *357* (1), 75-81.

22. Schulz, F.; Friedrich, W.; Hoppe, K.; Vossmeyer, T.; Weller, H.; Lange, H., Effective PEGylation of gold nanorods. *Nanoscale* **2016,** *8* (13), 7296-7308.

23. Burrows, N. D.; Lin, W.; Hinman, J. G.; Dennison, J. M.; Vartanian, A. M.; Abadeer, N. S.; Grzincic, E. M.; Jacob, L. M.; Li, J.; Murphy, C. J., Surface Chemistry of Gold Nanorods. *Langmuir* **2016,** *32* (39), 9905-9921.

24. Hanske, C.; Sanz-Ortiz, M. N.; Liz-Marzan, L. M., Silica-Coated Plasmonic Metal Nanoparticles in Action. *Adv Mater* **2018,** *30* (27): e1707003.

25. Janicek, B. E.; Hinman, J. G.; Hinman, J. J.; Bae, S. H.; Wu, M.; Turner, J.; Chang, H. H.; Park, E.; Lawless, R.; Suslick, K. S.; Murphy, C. J.; Huang, P. Y., Quantitative Imaging of Organic Ligand Density on Anisotropic Inorganic Nanocrystals. *Nano Letters* **2019,** *19* (9), 6308-6314.

26. Wu, M.; Vartanian, A. M.; Chong, G. N.; Pandiakumar, A. K.; Hamers, R. J.; Hernandez, R.; Murphy, C. J., Solution NMR Analysis of Ligand Environment in Quaternary Ammonium-Terminated Self -Assembled Monolayers on Gold Nanoparticles: The Effect of Surface Curvature and Ligand Structure. *J Am Chem Soc* **2019,** *141* (10), 4316-4327.

27. Ma, Z. Y.; LeBard, D. N.; Loverde, S. M.; Sharp, K. A.; Klein, M. L.; Discher, D. E.; Finkel, T. H., TCR Triggering by pMHC Ligands Tethered on Surfaces via Poly(Ethylene Glycol) Depends on Polymer Length. *Plos One* **2014,** *9* (11): e112292.

28. Sedlak, S. M.; Bauer, M. S.; Kluger, C.; Schendel, L. C.; Milles, L. F.; Pippig, D. A.; Gaub, H. E., Monodisperse measurement of the biotin-streptavidin interaction strength in a well-defined pulling geometry. *Plos One* **2017,** *12* (12): e0188722.

29. Abadeer, N. S.; Brennan, M. R.; Wilson, W. L.; Murphy, C. J., Distance and Plasmon Wavelength Dependent Fluorescence of Molecules Bound to Silica-Coated Gold Nanorods. *ACS Nano* **2014,** *8* (8), 8392-8406.

30. Egorova, E. A.; van Rijt, M. M. J.; Sommerdijk, N.; Gooris, G. S.; Bouwstra, J. A.; Boyle, A. L.; Kros, A., One Peptide for Them All: Gold Nanoparticles of Different Sizes Are Stabilized by a Common Peptide Amphiphile. *ACS Nano* **2020**, *14* (5), 5874-5886.

31. Korevaar, P. A.; Newcomb, C. J.; Meijer, E. W.; Stupp, S. I., Pathway selection in peptide amphiphile assembly. *J Am Chem Soc* **2014,** *136* (24), 8540-8543.

32. Orendorff, C. J.; Murphy, C. J., Quantitation of metal content in the silver-assisted growth of gold nanorods. *J Phys Chem B* **2006,** *110* (9), 3990-3994.

33. Shaw, C. P.; Middleton, D. A.; Volk, M.; Levy, R., Amyloid-derived peptide forms self-assembled monolayers on gold nanoparticle with a curvature-dependent beta-sheet structure. *ACS Nano* **2012,** *6* (2), 1416-1426.

34. Susi, H.; Byler, D. M., Resolution-Enhanced Fourier-Transform Infrared-Spectroscopy of Enzymes. *Method Enzymol* **1986,** *130*, 290-311.

35. Chirgadze, Y. N.; Nevskaya, N. A., Infrared-Spectra and Resonance Interaction of Amide-One Vibration of Parallel-Chain Pleated Sheet. *Biopolymers* **1976,** *15* (4), 627-636.

36. Kong, J.; Yu, S., Fourier transform infrared spectroscopic analysis of protein secondary structures. *Acta Bioch Bioph Sin* **2007,** *39* (8), 549-559.

37. Mei, B. C.; Oh, E.; Susumu, K.; Farrell, D.; Mountziaris, T. J.; Mattoussi, H., Effects of Ligand Coordination Number and Surface Curvature on the Stability of Gold Nanoparticles in Aqueous Solutions. *Langmuir* **2009,** *25* (18), 10604-10611.

38. Hendricks, M. P.; Sato, K.; Palmer, L. C.; Stupp, S. I., Supramolecular Assembly of Peptide Amphiphiles. *Acc Chem Res* **2017,** *50* (10), 2440-2448.

39. Shiraishi, K.; Yokoyama, M., Toxicity and immunogenicity concerns related to PEGylated-micelle carrier systems: a review. *Sci Technol Adv Mat* **2019,** *20* (1), 324-336.

40. Sahoo, J. K.; Braegelman, A. S.; Webber, M. J., Immunoengineering with Supramolecular Peptide Biomaterials. *J Indian I Sci* **2018,** *98* (1), 69-79.

41. Mikolajczak, D. J.; Heier, J. L.; Schade, B.; Koksch, B., Catalytic Activity of Peptide-Nanoparticle Conjugates Regulated by a Conformational Change. *Biomacromolecules* **2017,** *18* (11), 3557-3562.

4.7 Supporting Information

Thickness of the shell formed by **3** was determined from the TEM images:

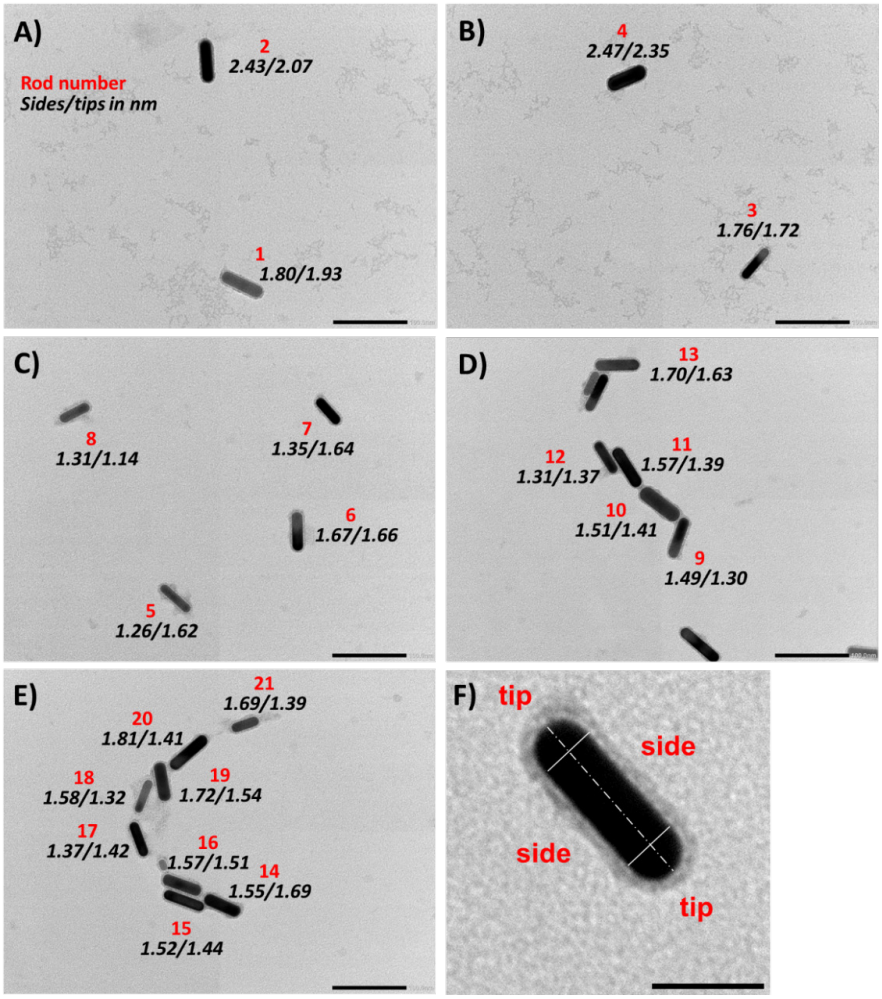

Figure S4.1. Analysis of the shell thickness of **GNR@3** as an example, based on the TEM images. Individual GNRs were numbered: (A) #1,2; (B) #3,4; (C) #5-8; (D) #9-13; (E) 14-21. To compare the shell thickness, the rod was divided as shown in (F). GNR numbers are shown in red, while the shell thickness is expressed in nm (first number indicates shell thickness at the sides of a rod, second number – at the tips). Negative staining was used to visualize the shells (0.5% uranyl acetate). Scale bar is 100 nm (A-E) and 25 nm (F).

Table S4.1. Analysis of the shell thickness derived from the TEM images of 21 individual GNRs. Mean parameters are given at the bottom of the table.

Rod #	Shell thickness, nm		SD*, nm		Ratio, %	
	sides	tips	sides	tips	sides	tips
1	1,80	1,93	0,23	0,28		107
2	2,43	2,07	0,19	0,23		85
3	1,76	1,72	0,21	0,25		98
4	2,47	2,35	0,25	0,29		95
5	1,26	1,62	0,19	0,23		128
6	1,67	1,66	0,30	0,30		100
7	1,35	1,64	0,23	0,19		121
8	1,31	1,14	0,19	0,22		87
9	1,49	1,30	0,24	0,32		87
10	1,51	1,41	0,39	0,30		93
11	1,57	1,39	0,40	0,31	100	89
12	1,31	1,37	0,30	0,29		104
13	1,70	1,63	0,32	0,38		96
14	1,55	1,69	0,31	0,59		109
15	1,52	1,44	0,37	0,21		95
16	1,57	1,51	0,29	0,34		96
17	1,37	1,42	0,26	0,26		104
18	1,58	1,32	0,44	0,46		84
19	1,72	1,54	0,36	0,34		89
20	1,81	1,41	0,28	0,29		78
21	1,69	1,39	0,27	0,32		82
av	1,64	1,57	0,29	0,30	100	97

* SD – standard deviation. The rod was divided into tips and sides as shown in **Figure S4.1F**.

Determination of coverage density provided by thiolated peptide amphiphiles:

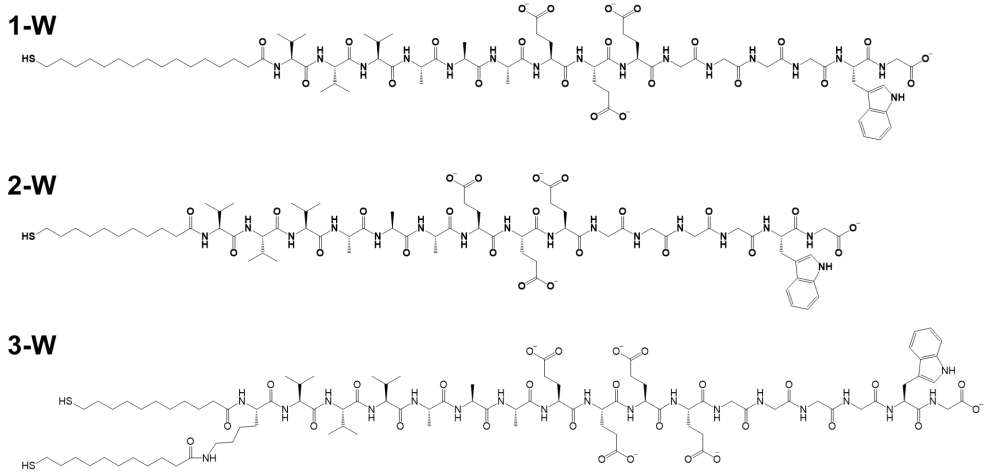

Figure S4.2. Chemical structures of thiolated peptide amphiphiles used to determine the coverage densities of the ligand on the GNR surface (46.4 by 14.0 nm, a.r. of 3.3): **1-W** was used to determine the coverage density of **1**, **2-W** – of **2**, **3-W** – of **3**.

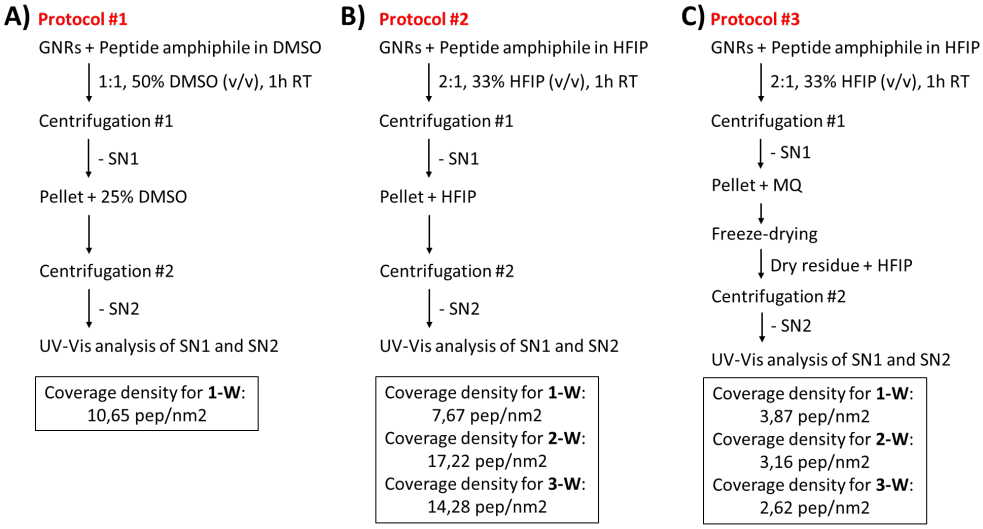

Scheme S4.1. Workflows illustrating the protocols tested to determine peptide amphiphile coverage density: (A) protocol #1, (B) protocol #2, and (C) protocol #3. Calculated coverage densities are given below the workflows.

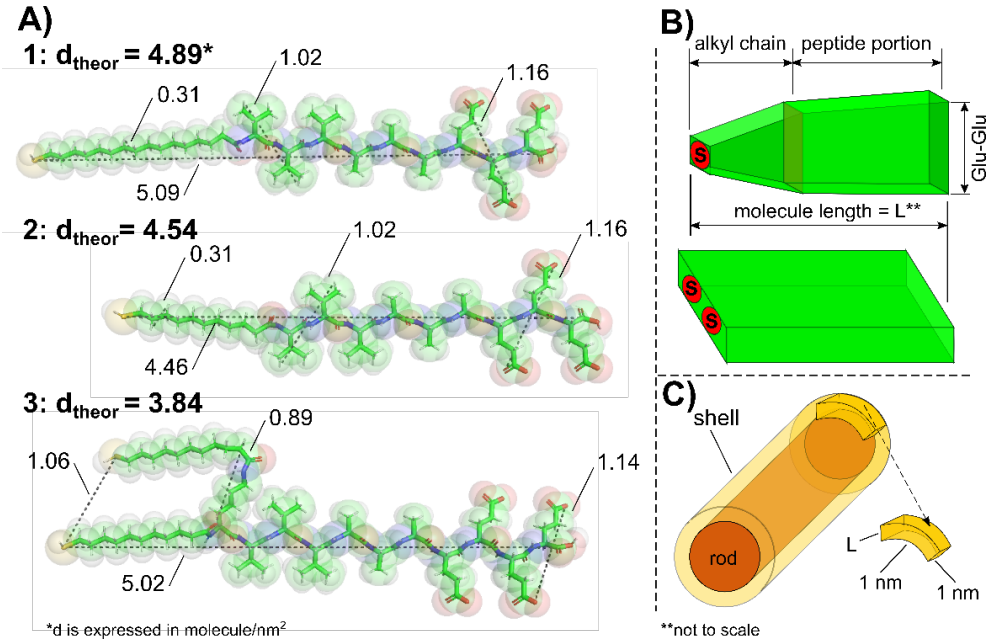

Scheme S4.2. Simulation of theoretical coverage density of peptide amphiphiles on a cylindrical surface: (panel A) contour length and possible dimensions of peptide amphiphile molecules **1-3**; (panel B) schematics illustrating simplified geometries given to molecule **1,2** (top) and **3** (bottom) to calculate the molecule volume; (panel C) a shell segment corresponding to 1 nm^2 of the gold surface occupied by 4.89 molecules of **1**, 4.54 molecules of **2**, or by 3.84 molecules of **3**. Theoretical coverage density (d_{theor}) was expressed as the ratio between the shell volume and the volume of one molecule. Models were built using PyMol. The dimensions are given in nm.

The following equations (2-11) describe how the d_{theor} values in **Scheme S4.2** were calculated.

Molecules **1** and **2** were simplified into two adjacent right frustums: one describing the alkyl chain and the other - the peptide segment (**Scheme S4.2**). The fully stretched molecules, as well as fully β-structured molecules, are flat and have a thickness corresponding to the alkyl chain (0.31 nm for all three molecules). Molecule volumes were calculated as follows:

$$V_{molecule} = V_I + V_{II}, \quad (2)$$

where $V_{molecule}$ is the volume of a molecule **1** or **2** (dimensions shown in **Scheme S4.2**), V_I is the volume of the alkyl chain, and V_{II} is the volume of the peptide segment.

$$V_I = {}^1\!/_3 \cdot L_I \cdot \left(S_1 + S_2 + \sqrt{S_1 \cdot S_2}\right), \quad (3)$$

where L_I is the distance between the sulfur atom and the amide bond formed due to the coupling of the alkyl chain to the N-terminus of the peptide segment (L_I = 2.11 nm for molecule **1** and L_I = 1.49 nm for molecule **2**); where S_1 is the (square) area with the alkyl chain distance in the base (S_1 = (0.31 nm)^2 for both molecules); S_2 is the (rectangular) area with the Val-to-Val distance in the base (S_2 = (1.02 nm) × (0.31 nm) for both molecules),

$$V_{II} = {}^1\!/_3 \cdot L_{II} \cdot \left(S_2 + S_3 + \sqrt{S_2 \cdot S_3}\right), \quad (4)$$

where L_{II} is the distance between the termini of the peptide segment (L_{II} = 2.98 nm for both molecules) and where S_3 is the (rectangular) area with the Glu-to-Glu distance in the base (S_3 = (1.16 nm) × (0.31 nm) for both molecules).

Molecule **3** was simplified in a different way: it was presented by a rectangular box with a base of $D_{alkyl\ chain}$ = 0.31 nm (the thickness of alkyl chain) by $D_{Glu-Glu}$ = 1.14 nm (Glu-to-Glu distance):

$$V_3 = L_{S-Cterm} \cdot D_{Glu-Glu} \cdot D_{alkyl\ chain}, \quad (5)$$

where $L_{S-Cterm}$ is the distance between the sulfur atom and the peptide C-terminus ($L_{S-Cterm}$ = 5.02 nm).

To calculated the shell volume V_{shell}, the volume of a gold rod segment V_{rod} and the volume of a coated rod segment $V_{rod+shell}$ were determined:

$$V_{rod} = \pi \cdot r_{rod}^2 \cdot h_{rod}, \quad (6)$$

where r_{rod} is the diameter of the rod (r_{rod} = 7.00 nm) and where h_{rod} is the rod length,

$$V_{rod+shell} = \pi \cdot (r_{rod} + L_{molecule})^2 \cdot h_{rod}, \quad (7)$$

where the length of the molecule $L_{molecule}$ is the distance between the sulfur atom and the C-terminus of the peptide segment (see **Scheme S4.2**). The shell volume is then:

$$V_{shell} = V_{rod+shell} - V_{rod}. \quad (8)$$

The lateral surface area of a rod is given by:

$$S_{lateral} = 2\pi \cdot r \cdot h_{rod}. \quad (9)$$

Next, we determine the number of molecules $N_{molecules}$ in a shell by dividing the shell volume by the volume of a single molecule:

$$N_{molecules} = {}^{V_{shell}}/_{V_{molecule}}. \quad (10)$$

Finally, the theoretical coverage density d_{theor} was calculated by dividing the number of molecules in a shell by the lateral surface area of a rod:

$$d_{theor} = {}^{N_{molecules}}/_{S_{lateral}} = {}^{L_{molecule}}/_{V_{molecule}} \cdot \left(1 + {}^{L_{molecule}}/_{2r_{rod}}\right). \quad (11)$$

The numerical values for the theoretical coverage density d_{theor} for the three types of molecule are presented in **Table S4.2**.

Table S4.2. Calculation of theoretical coverage densities for molecules 1-3 displayed on a cylindrical surface of 14 nm in diameter.

Molecule	$V_{molecule}$ (nm^3)	$L_{molecule}$ (nm)	d_{theor} (molecule/nm^2)
1	1.419	5.09	4.89
2	1.296	4.46	4.54
3	1.774	5.02	3.84

Self-assembly of the peptide amphiphile monolayer attached to the GNR surface:

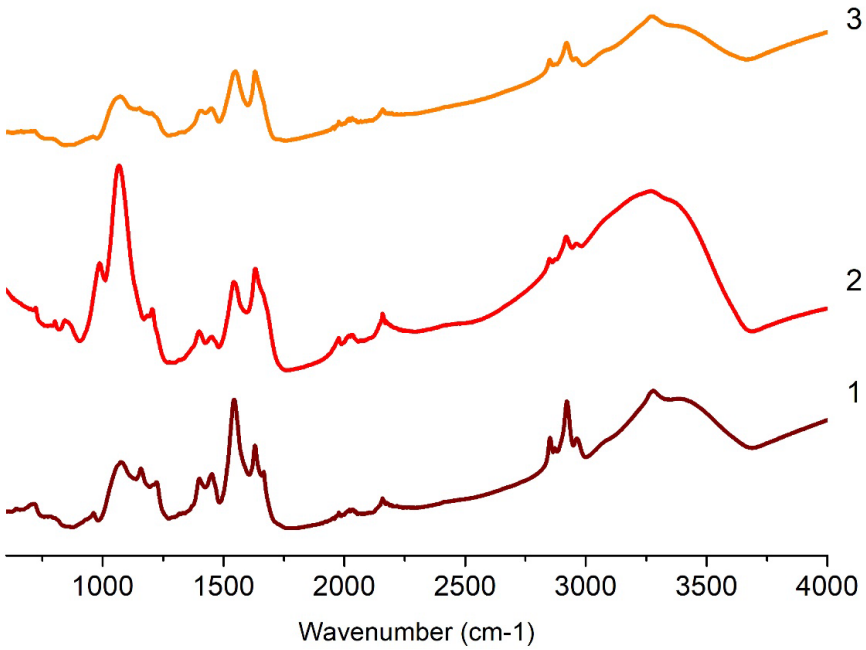

Figure S4.3. Full ATR-IR spectra of the coated GNRs with the thiolated peptide amphiphiles: brown line - **GNR@1**, red line - **GNR@2**, and orange line - **GNR@3**. Full FTIR-IR spectra for the corresponding peptide amphiphiles can be found in **Chapter 3**.

Table S4.3. Secondary structure distribution of peptide amphiphiles **1-3** in isolation and bound to the GNR surface.

Sample	β, %	Unordered, %	α, %	Others, %
1	97.7	0	0	2.3
GNR@1	58.8	3.9	14.8	22.5
2	85.2	0	5.4	9.4
GNR@2	51.8	6.0	20.5	21.7
3	94.8	0	0.8	4.4
GNR@3	57.1	6.8	19.0	17.1

The distribution is based on a fitting of Amide I peaks into 4 individual peaks and is shown as a percentage (deduced through area under the curve). Fitting into the Lorenz function were done using Origin Pro. ATR-IR spectra are shown in **Figure 4.4** and **Figure S4.3**.

GNR aggregation tests based on charge screening effects and competition with thiolated ligands:

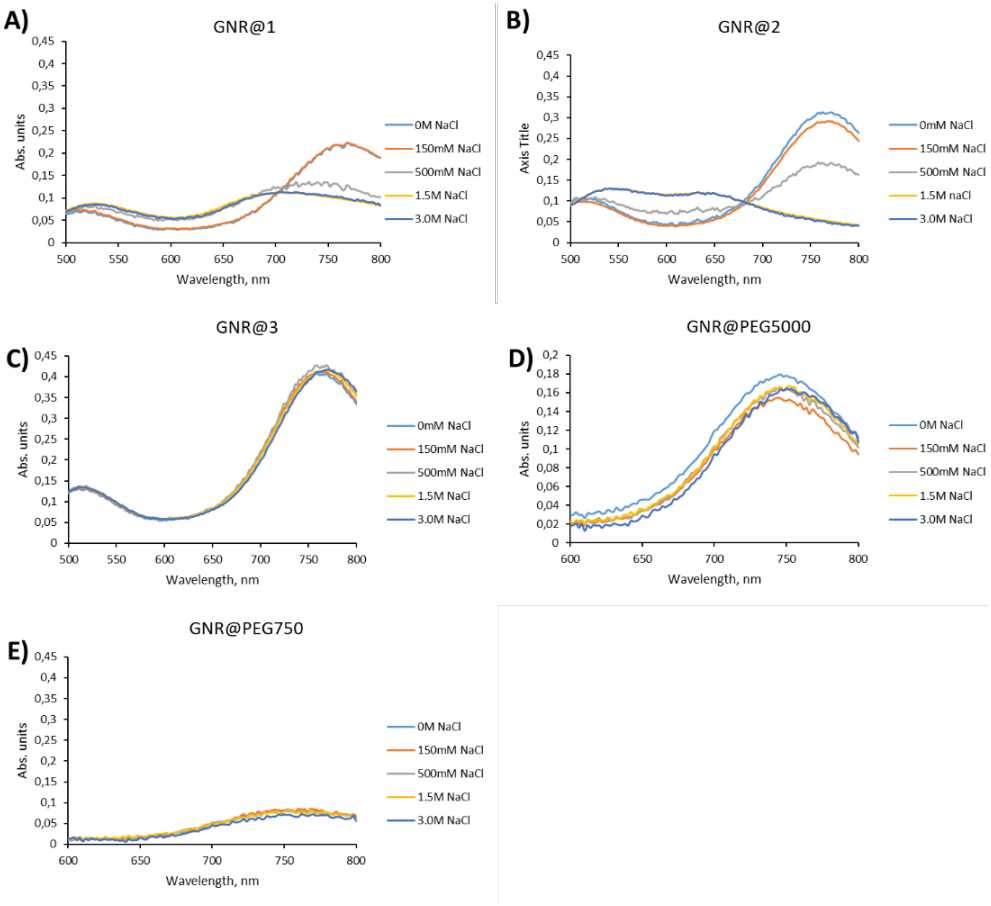

Figure S4.4. UV-Vis spectra recorded during the salt-induced aggregation assay for GNRs coated with (A) **1**; (B) **2**; (C) **3**; (D) **PEG$_{5000}$**; (E) **PEG$_{750}$** used to obtain normalized aggregation factor (AF). Coated GNRs (originally dispersed in MilliQ water) were mixed with NaCl to yield final salt concentrations of: 150 mM (orange line), 500 mM (gray line), 1.5 M (yellow line), and 3.0 M (blue line). After mixing, samples were incubated 15 min at room temperature. The sample with no salt added (0 M NaCl, light blue line) served as a reference to calculate AF (for results, see **Figure 4.5**). Measurements were carried out at room temperature.

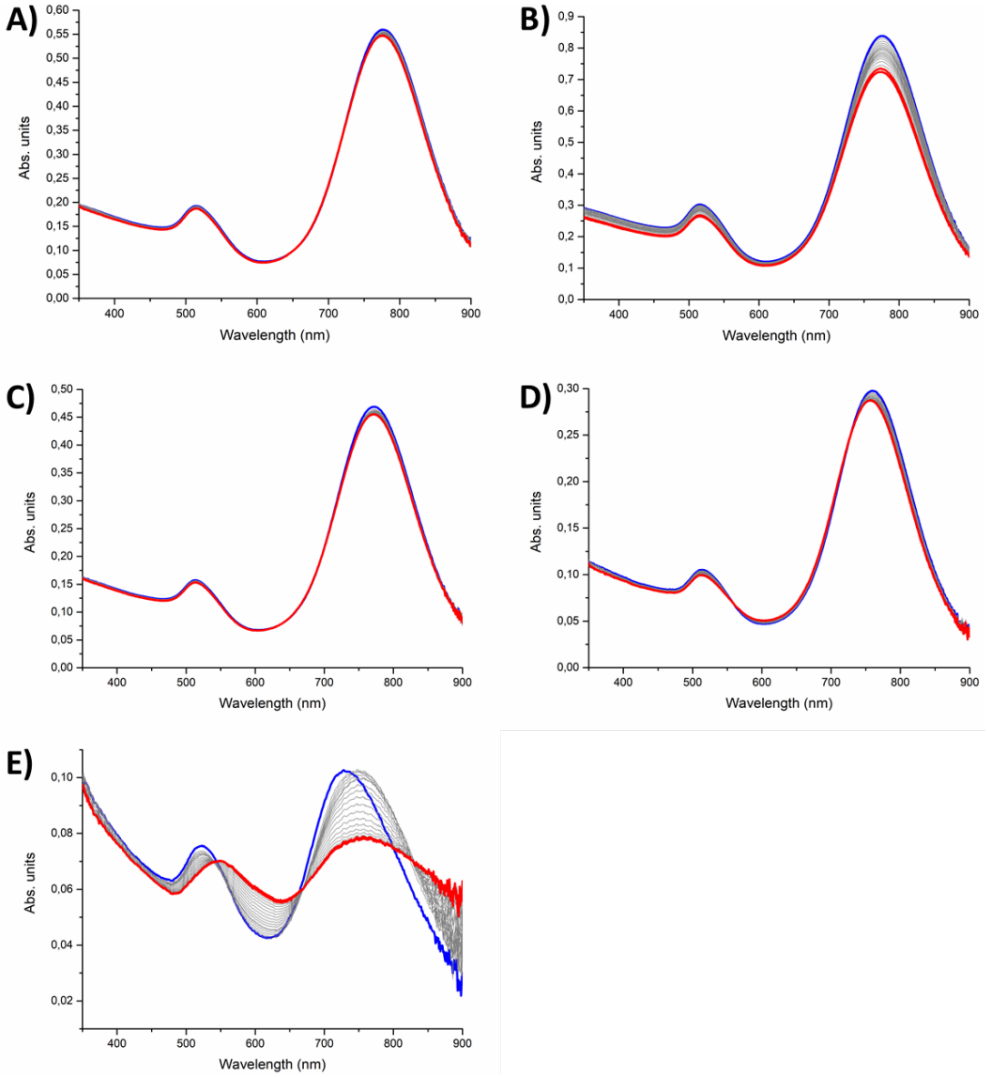

Figure S4.5. UV-Vis spectra recorded during the DTT competition assay to obtain normalized aggregation factor (AF) for GNRs coated with: (A) **1**; (B) **2**; (C) **3**; (D) **PEG$_{5000}$**; (E) **PEG$_{750}$**. Coated GNRs (originally dispersed in MilliQ water) were mixed with DTT to yield a final DTT concentration of 1 M (blue line, t = 0 min), a UV-Vis spectrum was recorded every 5 mins (gray lines) over a course of 90 mins (red line, t = 90 mins). The sample at t = 0 min (blue line) served as a reference to calculate AF (for results, see **Figure 4.5**). Measurements were carried out at room temperature.

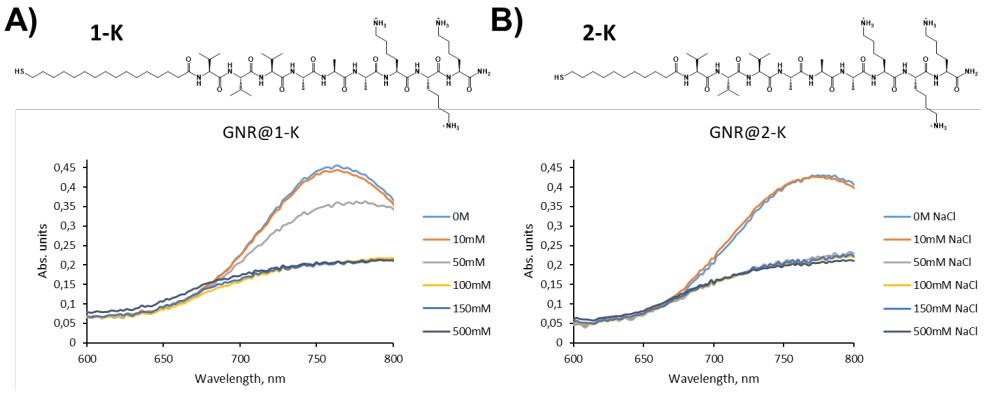

Figure S4.6. Salt-induced aggregation of GNRs coated with positively charged peptide amphiphiles was monitored with UV-Vis spectroscopy to obtain normalized aggregation factor (AF) for GNRs coated with (A) **1-K** and (B) **2-K**. Coated GNRs (originally dispersed in MilliQ water) were mixed with NaCl to yield final salt concentrations of: 10 mM (orange line), 50 mM (gray line), 100 mM (yellow line), 150 M (blue line), and 500 mM (dark gray line). After mixing samples were incubated 15 min at room temperature. The sample with no salt added (0 M NaCl, light blue line) served as a reference to calculate AF (for results, see **Figure 4.6**). Measurements were carried out at room temperature. Chemical structures of **1-K** and **2-K** are shown above the UV-Vis spectra.

Characterization of the synthesized peptides and peptide amphiphiles by LC-MS:

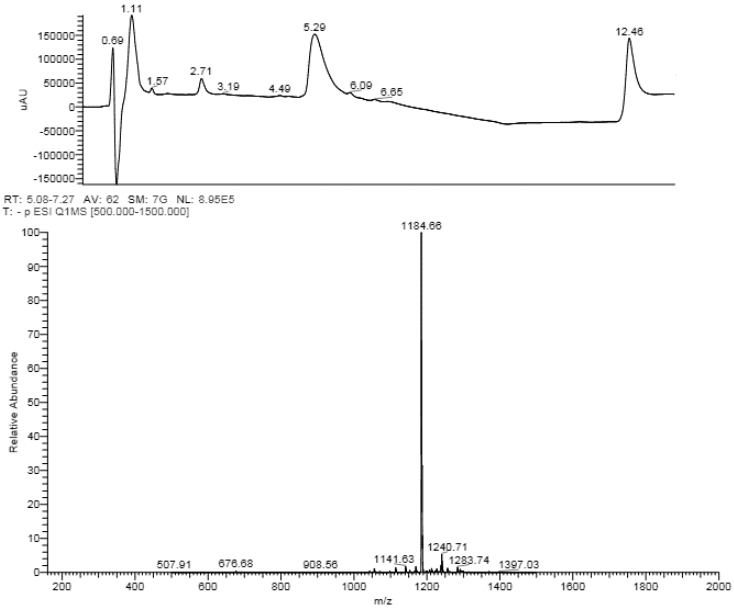

Figure S4.7. LC-MS spectrum for **1**. $[M\text{-}H]^{1-}_{theor}$ =1184.65.

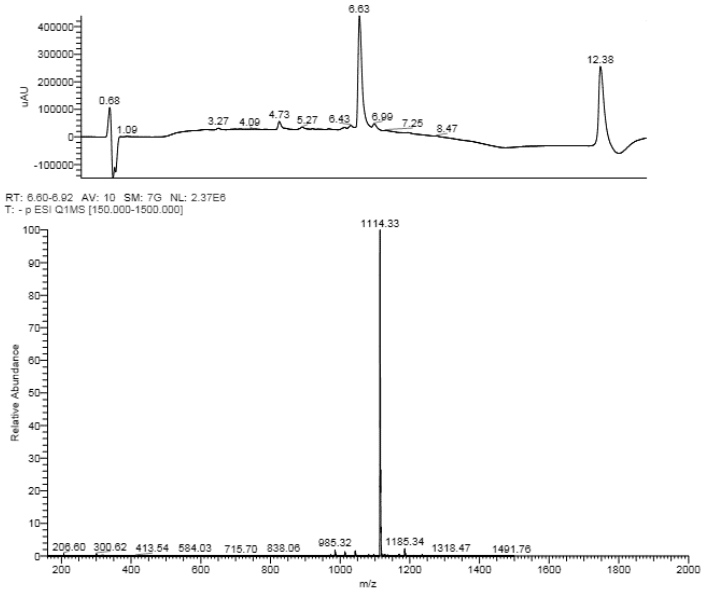

Figure S4.8. LC-MS spectrum for **2**. $[M\text{-}H]^{1-}_{theor}$ =1114.57.

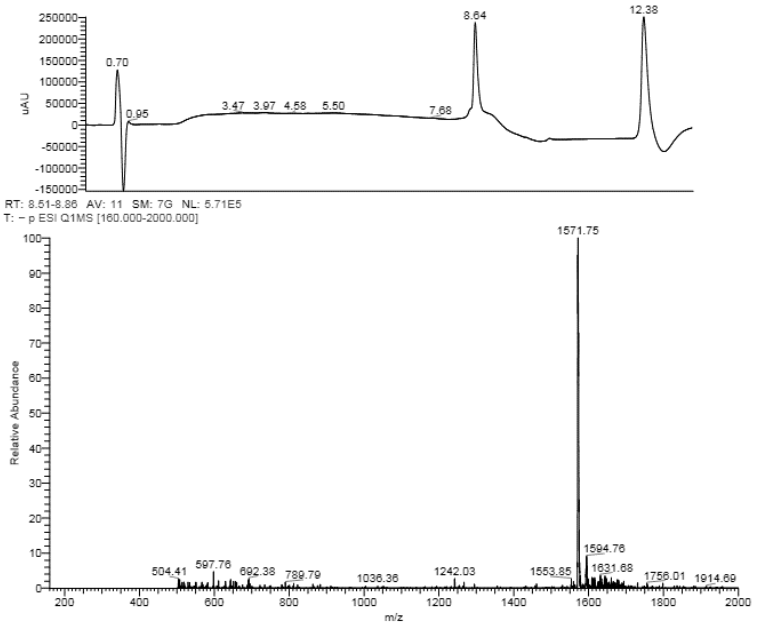

Figure S4.9. LC-MS spectrum for **3**. $[M\text{-}H]^{1-}_{theor}$ =1571.83.

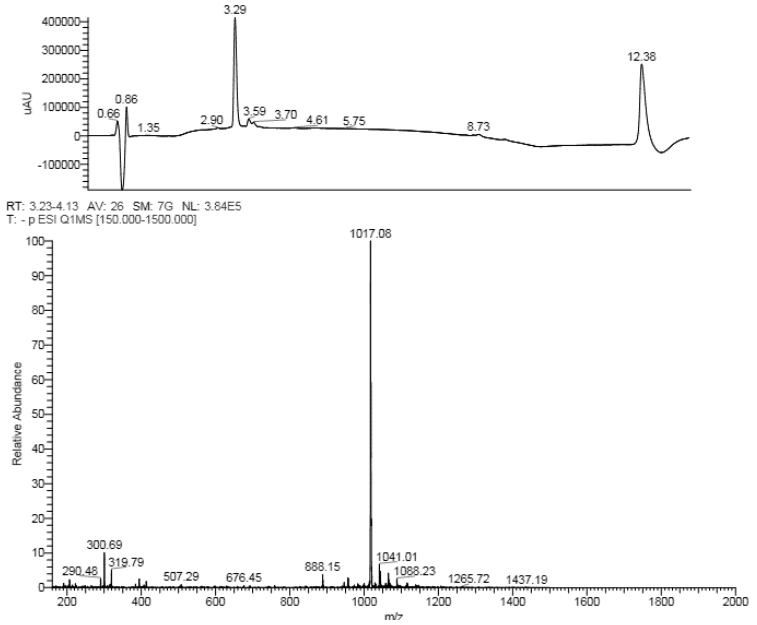

Figure S4.10. LC-MS spectrum for **4**. $[M\text{-}H]^{1-}_{theor}$ =1017.45.

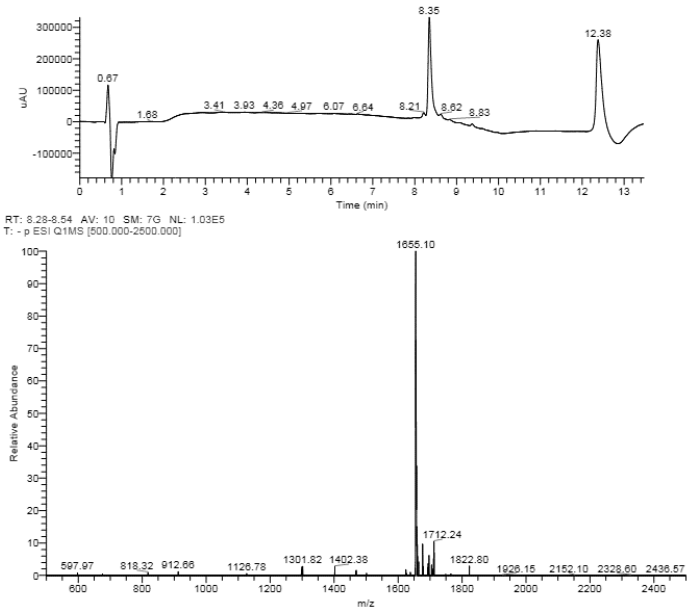

Figure S4.11. LC-MS spectrum for **1-W**. $[M-H]^{1-}_{theor}$ =1654.82.

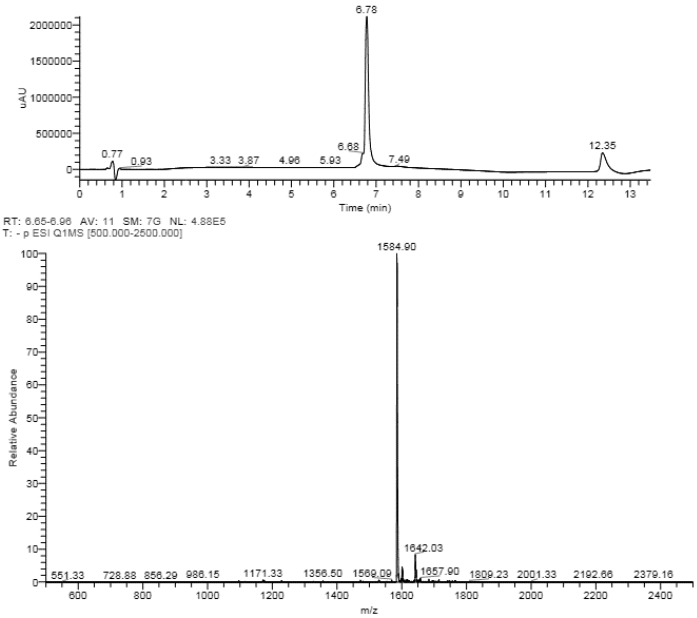

Figure S4.12. LC-MS spectrum for **2-W**. $[M-H]^{1-}_{theor}$ =1585.75.

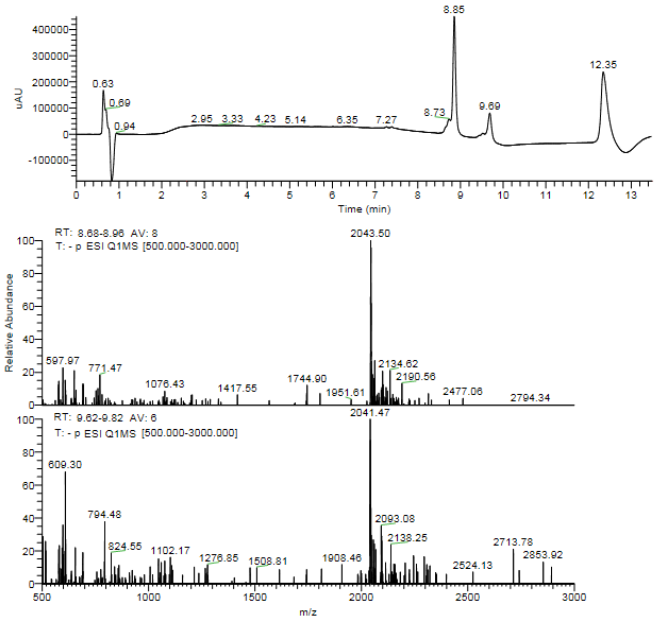

Figure S4.13. LC-MS spectrum for **3-W**. $[M-H]^{1-}_{theor}$ =2043.03; for the dimeric species $[M-2H]^{2-}_{theor}$ = 2041.50.

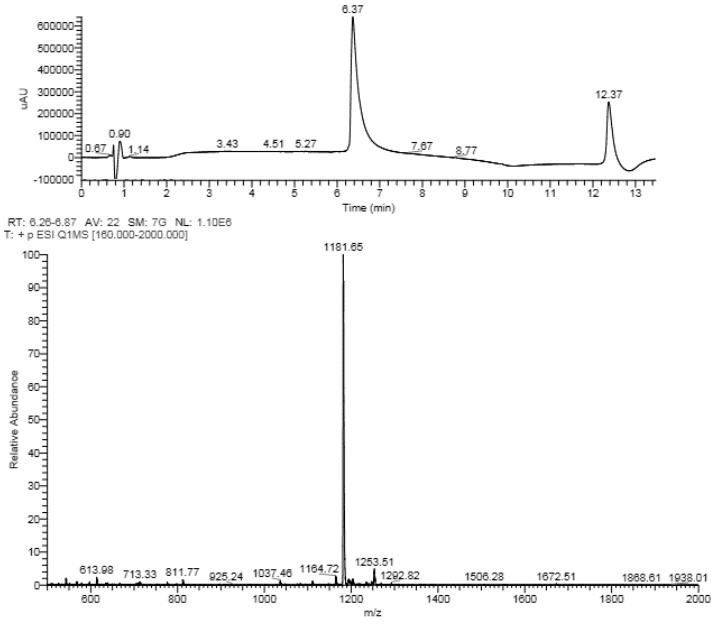

Figure S4.14. LC-MS spectrum for **1-K**. $[M+H]^{1+}_{theor}$ =1181.83.

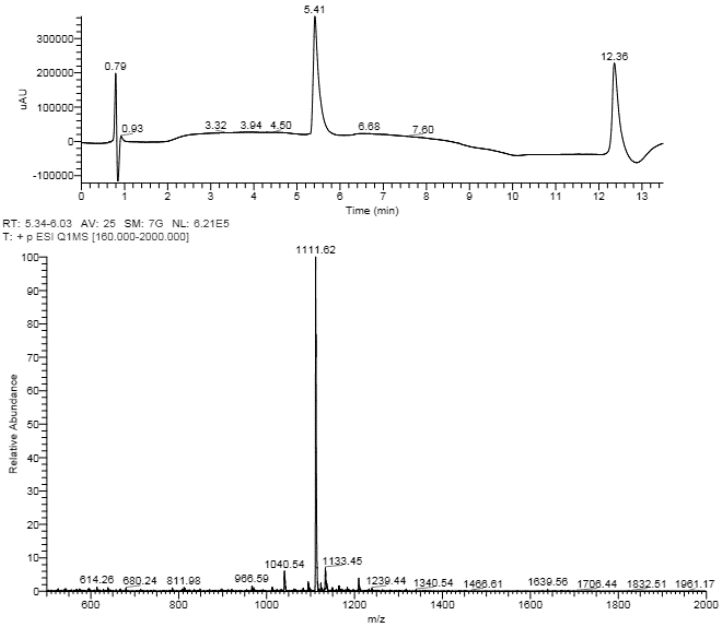

Figure S4.15. LC-MS spectrum for **2-K**. $[M+H]^{1+}_{theor}$ = 1111.75.